Int J Clin Exp Pathol 2021;14(2):267-291
www.ijcep.com /ISSN:1936-2625/IJCEP0124033

Original Article

Knockdown of KIF15 promotes cell apoptosis by activating crosstalk of multiple pathways in ovarian cancer: bioinformatic and experimental analysis

Xinwei Sun[1], Mengyue Chen[2], Bin Liao[3], Zhiqing Liang[1]

[1]*Department of Gynecology and Obstetrics, Southwest Hospital, Army Medical University, Chongqing, China;*
[2]*Department of Gynecology and Obstetrics, The First People's Hospital of Liang Jiang Area, Chongqing, China;*
[3]*Department of Neurosurgery, Chongqing General Hospital, University of The Chinese Academy of Sciences, Chongqing, China*

Received October 13, 2020; Accepted December 8, 2020; Epub February 1, 2021; Published February 15, 2021

Abstract: Background: Ovarian cancer (OC) is the most lethal malignancy of women. Unlimited proliferation is a fundamental feature of OC cells. The genes associated with cell proliferation may be histopathologic biomarkers and targets of anti-tumor therapeutic strategies. The present study aimed to identify proliferation-associated biomarkers with prognostic, diagnostic, and therapeutic value and reveal the underlying molecular mechanism of candidate genes involved in OC by a combination of bioinformatic and experimental methods. Results: KIF15 was upregulated in early-stage OC tissues and could predict poor prognosis of patients of Stage I and II. The knockdown of KIF15 significantly inhibited cell proliferation, tumor formation, and growth as well as promoting apoptosis of OC cells. A combination of experimental and bioinformatic analyses revealed KIF15 knockdown promoted cell apoptosis by activating crosstalk of multiple pathways in OC. Conclusion: KIF15, an early-stage prognostic gene, was identified as a candidate histopathologic biomarker and therapeutic target of OC.

Keywords: Ovarian neoplasms, kinesin, prognosis, early diagnosis, molecular targeted therapy, cell proliferation, apoptosis

Introduction

OC ranks as the most lethal tumor in female reproductive organs. The incidence of this gynecological malignancy has been continuously increasing each year. In 2018, there were approximately 22,240 newly diagnosed OC cases and 14,070 deaths of OC in the United States [1]. The poor prognosis of OC is mainly due to the lack of reliable diagnostic and prognostic biomarkers especially in early stages. The two serum biomarkers of OC, Cancer Antigen 125 (CA125) and Human Epididymis Protein 4 (HE4), are used to detect the fatal disease. Although the specificity of CA125+ HE4 reaches to 82.85% and the sensitivity is 92.18%, their combined use does little for early diagnosis and prognosis of OC [2]. Thus, although surgical techniques have been improved and new chemotherapeutic agents such as PARP inhibitors [3] have been applied to clinical treatment, the improvement of OS in OC patients is still unsatisfactory. Biomarkers of early prognostic indicators are needed, as well as novel histopathologic diagnostic biomarkers and therapeutic targets.

With genomic technologies rapidly developing in recent years, large amounts of high-throughput data have been generated. Genome-wide RNA expression analysis has become a frequently-used tool for researchers to screen and understand genes that play key roles in tumorigenesis and progression. A variety of high-throughput platforms such as GEO [4] and the Cancer Genome Atlas (TCGA) [5] can identify genes that might serve as early prognostic and histopathological biomarkers or even contribute to targeted therapy. Also, integrated analysis by multiple bioinfomatic methods can also provide crucial clues for a better understanding of the molecular mechanism of candidate genes involved in a certain tumor.

Researchers have focused on identifying prognostic and diagnostic biomarkers as well as therapeutic targets of OC by bioinformatic methods. Being an important part of tumor growth and progression, proliferation-associated genes have been considered diagnostic and therapeutic targets for years [6]. Multiple previous bioinformatic studies have confirmed that proliferation-associated genes are an important component of differentially expressed genes (DEGs) screened between normal ovarian and OC tissues. In a bioinformatic study using GEO datasets, researchers found that up-regulated DEGs between normal and OC tissues were mainly enriched in the GO category of cell proliferation [7]. Another study reported that up-regulated DEGs between normal and OC samples were mainly associated with cell cycle and cell division, which were also closely related to cell proliferation. Four genes (BUB1B, BUB1, TTK and CCNB1) were then identified as proliferation-associated biomarkers with prognostic value [8]. Furthermore, by using topologic methods, researchers obtained 6 hub genes (DTL, DLGAP5, KIF15, NUSAP1, RRM2, and TOP2A) among the DEGs from OC datasets, all of which were strongly linked to cell cycle and cell division [9]. A similar study also reported that three proliferation-associated gene BUB1B, KIF20A, and KIF11 were hub genes with both prognostic value of OS and PFS [10], further indicating the crucial role of cell proliferation. As shown above, different datasets and bioinformatic methods used in the study as well as varying researchers' interests may generate novel biomarkers, which is a vital characteristic of high throughput data mining. However, no matter what data-processing methods, analytical tools and gene screening criteria the researchers use, proliferation-associated genes are an important part of the OC DEGs compared to normal tissues. Thus, we expect that we can obtain therapeutic targets with an early prognostic and histopathologic diagnostic value from the proliferation signatures to better understand the pathogenesis and to improve the survival of OC. To identify more reliable biomarkers, an integrated bioinformatic analyses combined with experimental verification should be performed.

In the present research, we identified 40 proliferation-associated genes from 190 consistent DEGs between ovarian cancer and non-tumor specimens by analyzing the gene expression profiling of four GEO datasets. The Kalplan-Meier Plotter [11] was used to identify survival-related candidate genes. Thus, we obtained only two genes (KIF15 and BUB1 Mitotic Checkpoint Serine/Threonine Kinase B [BUB1B]) that were overexpressed and had a significant effect on OS in early-stage OC patients. Otherwise, we found KIF15 had a higher expression level in early stages than that of late stages, suggesting it may be an early-stage histopathologic biomarker for prognosis and diagnosis. Therefore, KIF15 was selected to be bioinformatically and functionally analyzed subsequently. Our study confirmed that KIF15 was a proliferation-associated gene useful in early prognosis and diagnosis of OC. Knockdown of KIF15 activated OC cell apoptosis through crosstalk among multiple pathways, indicating the possibility for KIF15 to be a therapeutic target in OC. These findings can provide reliable evidence for early diagnosis, prognosis and development of targeted therapies in OC.

Material and methods

Ethical statement

All animal experiments are in accordance with the "Regulations on the Administration of Laboratory Animals" (The National Science and Technology Commission of the People's Republic of China, March 1, 2017, revised edition) and the National Institutes of Health Laboratory Animal Care and Use Guidelines (ISBN: 13: 978-0-309-15400-0, revised in 2011) to ensure the animal welfare of experimental animals. This study was approved by the Human Research Ethics Committees of Southwest Hospital, Army Medical University (AMU).

OC datasets selection from the GEO database

We selected and downloaded the raw data of four OC datasets from the GEO database. GSE40595 [12] contained 63 high grade serous ovarian cancer samples and 14 normal ovarian samples. GSE18520 [13] contained 53 advanced stage, high-grade primary tumor samples, and 10 normal ovarian samples. GSE38666 [14] contained 25 serous ovarian cancer samples and 20 para-cancer samples. GSE36668 [15] contained 4 serous ovarian borderline tumor samples, 4 well-differentiated serous ovarian carcinomas, and 4 normal

ovarian samples. The four datasets were all based on the platform GPL570 (Affymetrix Human Genome U133 Plus 2.0 Array) to reduce variability from the different experimental setups. Quality analysis was performed on raw data of the selected GEO datasets respectively by using the affyPLM package [16] in R software. Three tumor samples in GSE40595, one tumor sample in GSE18520, and one tumor sample in GSE38666 datasets were removed from the data processing because of variance of sample quality. Thus, there were 155 tumor samples and 57 non-tumor samples included in our subsequent analysis in total.

Identification of proliferation-associated genes from the DEGs

To screen the DEGs in each GEO dataset, the limma package [17] was used with cutoff criteria of |log2 Fold Change (FC)| > 1.5 and adjusted *p*-value<0.05. The heatmaps were drawn by the tools in the Omicshare platform (https://www.omicshare.com/). For visualization, an online Venn diagram tool (http://bioinformatics.psb.ugent.be/webtools/Venn/) was used to show the overlapping part of DEGs in the four GEO datasets. The GO and Kyoto Encyclopedia of Genes and Genomes (KEGG) analysis was conducted by DAVID (Resource 6.8) [18]. The top 10 GO categories with the smallest *p*-value and the genes in five proliferation-associated categories ("cell division", "mitotic nuclear division", "cell proliferation", "mitotic sister chromatid segregation", "chromosome segregation") were visualized by GOplot package in R [19]. The results of pathway enrichment analysis were visualized by using Omicshare tools.

Identification of candidate genes with early prognostic value

The overall survival analysis of the proliferation-associated genes was conducted by the Kaplan-Meier Plotter in all OC patients in the database. To obtain genes with more significant prognostic value, *P*<0.01 was set as the screening criterion. Survival analysis was also performed on the previously obtained prognostic genes only in Stage I-II patients with a cutoff of *P*<0.05. The different expression among stages of the selected genes with early-stage prognostic value was analyzed in the Gene Expression Profiling Interactive Analysis (GEPIA) database [20]. KIF15 was selected to be bioinformatically analyzed and functionally verified in a subsequent study.

Bioinformatic verification of the expression level of KIF15 in normal and OC tissues

The RNA-seq data of the OC samples in TCGA and normal ovarian samples in GTEx were downloaded from the UCSC Xena project (https://xena.ucsc.edu/). The OC samples (N=379 for cystic, mucinous, and serous neoplasms) were limited to RNA-seq data of FPKM with HTseq and the GTEx samples (n=88 for normal ovarian tissue) were limited to RNAseq data of FPKM. The downloaded RNA-Seq data of both datasets have been recomputed to minimize differences from distinct sources based on a standard pipeline. The corresponding clinical information of the OC dataset was downloaded from the TCGA database (https://portal.gdc.cancer.gov/). The data of KIF15 expression in multiple normal tissue samples of females were extracted and visualized by the ggpubr package in R. The differential expression of KIF15 was visualized by the beeswarm package in R. The analysis of KIF15 differential expression in five kinds of female-specific malignancies was conducted by the GEPIA online tool. The RNA-seq data of KIF15 expression in ovarian cancer cell lines were downloaded from the Cancer Cell Line Encyclopedia (CCLE, https://portals.broadinstitute.org/ccle) [21].

Immunohistochemistry on OC tissue microarray

The tissue microarrays (Alenabio, Xi'an, China) used in the study contained a total of 100 samples, including 80 ovarian cancer tissue samples of different histologic types, 10 lymph node metastasis samples, and 10 non-tumor ovarian samples. Anti-KIF15 rabbit polyclonal antibody (Sigma-Aldrich Cat# HPA035517) was used to conduct the immunohistochemical staining at a dilution of 1:100. The positive staining was quantified and classified into 5 levels: negative staining for 0 score; 1%-25% positive staining cells was scored as 1; 26%-50% positive was a 2; 51%-75% positive was a 3 and 76%-100% positivewas a 4. Staining intensity was scored as negative (0), weak (1), moderate (2), and robust (3). All the pathologic sections were independently reviewed by two

pathologists and the expression levels were graded by the product of positive staining percentage score and staining intensity score.

Cell culture

The cell lines used in the study, including ovarian cancer cell lines SKOV3, OVCAR-3, A2780, and HO8910, cervical cancer cell lines Hela, Siha and C33A, lung adenocarcinoma cell line A549, pancreatic cancer cell line PANC-1 and glioblastoma cell line U87, were all purchased from the cell bank of Chinese Academy of Science (Shanghai, China). The cell lines were cultured according to the instructions online (http://www.cellbank.org.cn/).

Lentivirus transfection

Human KIF15 knocking down (KD) lentiviruses and negative control (NC) lentiviruses were constructed by Genechem (Shanghai, China). SKOV3 and HO8910 cells were seeded in 6-well plates the day before transduction to ensure the cells would grow to 30% to 40% confluence the next day, and then infected with lentivirus for 24 h at a Multiplicity of Infection (MOI) of 20 and 10 respectively in the presence of polybrene (5 mg/mL, Genechem).

qRT-PCR analysis

The qRT-PCR was performed as previously reported [22]. The $2^{\Delta\Delta cT}$ method was used to determine the expression of the KIF15 gene. All experiments were carried out in triplicate. The primers were purchased from Sangon Biotech (Shanghai, China).

KIF15: Forward 5'-CTCTCACAGTTGAATGTCCTTG-3'; Reverse 5'-CTCCTTGTCAGCAGAATGAAG-3'; GAPDH: Forward 5'-TGACTTCAACAGCGACACCCA-3'; Reverse 5'-CACCCTGTTGCTGTAGCCAAA-3'.

Western blot analysis

Western blot was performed as previously described [22]. GAPDH was used as a loading control. The KIF15 rabbit polyclonal antibody (1:100) and GAPDH monoclonal antibody (1: 1000, Santa Cruz Biotechnology Cat# sc-32233) were used.

Cell growth analysis by Celigo method

SKOV3 and HO8910 cells were transfected with KIF15-KD or NC lentivirus. The transfected cells were collected and then seeded into 48-well plates, 2000 cells per well respectively. The number of cells with green fluorescence in each well was measured by a Cellomics ArrayScan System (Nexcelom, USA) once a day. The variable data of the green fluorescence signal were obtained for statistical analysis to construct 5-day cell proliferation curves. The green-fluorescence cells were also scanned to be counted by image analysis software. The count of green-fluorescence cells at each time point was compared with that of day 1 to calculate the cell proliferation ratio for each time point and each experimental group. The fold change of cell proliferation was obtained to construct cell growth curves.

The cell proliferation ratio was computed as follows: fold change (NC vs. experimental group) = proliferation ratio on day 5 for the NC group/ proliferation ratio on day 5 for the experimental group. A fold change of proliferation ratio equal to or greater than 2 indicated that cell proliferation was significantly slowed.

Cell counting Kit-8 (CCK8) assay

SKOV3 and HO8910 cells were plated into 96-well plates at 2000 cells per well and transfected with the KIF15-KD or NC lentivirus. Cell proliferation was measured by using CCK8 Reagent (DOJINDO, Japan) respectively on days 1, 2, 3, 4, and 5 after transfection. The assays were performed in triplicate.

FACS assay by flow cytometry

Cells were seeded into 6-well plates and cultured in serum-free medium at 37°C for 24 h. Cells were transfected with the KIF15-KD or NC lentiviruses. Then the cells were harvested and analyzed by an AnnexinV-APC apoptosis kit (eBioscience, USA). Apoptosis was determined using the Guava InCyte software (Millipore, USA). All experiments were conducted in triplicate.

Caspase 3/7 activity assay

To assess the activity of caspases 3 and 7, the Caspase-Glo 3/7 Assay (Promega, Germany) was conducted following the manufacturer's instructions. The Caspase-Glo 3/7 Assay is based on the cleavage of the DEVD sequence of a luminogenic substrate by the caspases 3 and 7 and results in a luminescent signal. The fluorescence signal was measured at an excita-

tion wavelength of 485 nm and an emission wavelength of 527 nm.

Subcutaneous transplantation of human OC cells in Balb/c nude mice

Female Balb/c nude mice of four weeks old were used in this experiment. A total of 2×10^7 transfected SKOV3 cells were subcutaneously injected into the right armpit of each mouse. The body weight and tumor diameter of each mouse were measured every week after cell transplantation. All mice were sacrificed on the 41st day after cell injection. Before the mice were killed, the fluorescence images of xenograft tumors were photographed under a whole-body fluorescent imaging system (Lumina LT, Perkin Elmer, USA). Tumors were observed by both gross and microscopic methods.

mRNA expression profiling

The SKOV3 cells of KIF15-KD and NC group were collected for mRNA expression profiling. Total RNA was isolated from cell samples by using an Agilent RNA 6000 Nano Kit (Agilent, USA), and the quality of total RNA was analyzed. Both the KIF15-KD and NC cell samples had three replicates. The mRNA expression profiling was conducted by using GeneChip prime view humans (901838, Affymetrix, USA). RNA labeling and hybridization were performed with a GeneChip Hybridization Wash and Stain Kit (Agilent, USA). The raw data obtained from mRNA expression profiling was quality-analyzed using R software as in the aforementioned methods in Paragraph 2.2 before subsequent bioinformatic analysis.

Phospho-antibody arrays

To avoid batch difference, the same cell samples used for mRNA expression profiling were examined in this assay. The cell lysates of KIF15-KD and NC group were obtained and applied to a Cancer Signaling Phospho-Antibody Array (PCS300, Full Moon Biosystems, USA). The phosphoantibody array detection was carried out in cooperation with Wayne Biotechnology (Shanghai, China) per the manufacturer's protocol. The array contained 157 site-specific and phospho-specific antibodies and 147 non-phospho antibodies, each of which had 6 replicates. The slides were scanned by a GenePix 4000 scanner and the images were analyzed with GenePix Pro 6.0 (Molecular Devices, Sunnyvale, CA). The intensity of the fluorescence signal obtained from each antibody-stained region indicated the expression level of a certain protein. The extent of protein phosphorylation was measured by a ratio computation. The phosphorylation ratio was calculated as follows: phosphorylation ratio = phospho value/non-phospho value [23]. The total proteome ratios were standardized to β-actin.

Pathway analysis by multiple bioinformatic methods

The DEGs in mRNA expression profiling were obtained by using R packages with a cutoff of $|\text{Fold Change}| \geq 1.5$ and $P<0.05$. The pathway analysis was performed with the plug-in ClueGO [24] in Cytoscape software (Version 3.7.1) with a cutoff of $P<0.05$. GSEA (Version 3.0), a pathway enrichment method was also used to analyze a level of gene sets. GSEA software uses the predefined gene sets from the Molecular Signatures Database (MSigDB v6.2) [25]. A gene set is a group of genes that share similar pathways, functions, chromosomal localization, or other features. In this study, we used all the C collection sets for GSEA analysis (i.e., H, C1-C7 collection in MsigDB). The list of ranked genes based on a score calculated as -log10 of *p*-value multiplied by the sign of fold change. The minimum and maximum criteria for the selection of gene sets from the collection were 10 and 500 genes, respectively. Pathway enrichment analysis on the results of the phospho-antibody arrays was also performed. According to the pathways obtained by using DAVID and GSEA, the phosphorylated proteins on the pathways were selected and the protein-protein interactive (PPI) networks were visualized by Cytoscape. The consistent genes and phosphorylated proteins on the previously obtained pathways both in mRNA expression microarrays and phospho-antibody arrays were visualized by Venn tools in the Omicshare platform.

Statistical analysis

SPSS 20.0 (IBM SPSS, Chicago, IL) software was used for statistical analyses. Values are presented as the mean ± SD. Wilcox test was used to determine a significant expression dif-

ference of DEGs among ovarian cancer and non-tumor samples in GEO and TCGA datasets. The differences between NC and KD groups in proliferation and apoptosis assays were tested by the Student's t-test. The different expression levels between the ovarian cancer tissue samples and adjacent non-tumor samples in TMA were tested with the Mann-Whitney test. $P<0.05$ was considered significant.

Results

Identification of differentially expressed genes (DEGs) from GEO datasets of OC

In the present study, a multistep analysis was carried out to identify candidate genes modulating a certain biologic process. First, we selected four GEO datasets of mRNA expression profiling including ovarian cancer and non-tumor ovarian tissue samples. Because of the insufficiency of paracancer tissue in OC, the unpaired non-tumor ovarian tissue was used to replace the paired paracancer tissue. After removing the unqualified samples (Figure S1), 155 tumors and 57 non-tumor samples were included in the subsequent analyses. Second, we aimed to screen DEGs in each GEO dataset with the criteria of log2 (**Figure 1A-D**). Consequently, 190 consistent genes, including 183 upregulated, and 7 downregulated genes were obtained from the four GEO datasets (**Figure 1E**, **1F**).

Functional annotation and pathway enrichment analysis of the consistent DEGs

GO and KEGG analysis of the 190 DEGs was conducted by DAVID. The ten BP categories with the smallest adjusted *p*-value were shown in **Figure 1G**. Five proliferation-associated BP categories were selected and the genes enriched to the categories were shown in the circle plot (**Figure 1H**). Thus, forty proliferation-associated genes were screened. We obtained 17 genes simultaneously enriched to two or more categories of the five proliferation-related ones (SAC3D1, NUF2, FAM83D, TPX2, KIF11, ZWINT, CDCA3, NDC80, PTTG1, BUB1B, KIF15, KI, F18B, SPAG5, CENPF, CDC20, CDK1, and KIF2C), which strongly indicated they were the hub genes and key nodes in the biological process of proliferation. The results of pathway enrichment analysis were shown in **Figure 1I**.

Identification of survival-related genes

Survival analyses of the 17 selected genes were performed by Kaplan-Meier Plotter. To obtain genes with more significant prognostic value, we selected overall survival-associated genes with a cutoff of $P<0.01$. The overall survival curves of the six genes (BUB1B, CDK1, CENPF, FAM83D, KIF15, and TPX2) with significant prognostic value are shown (**Figure 2A-F**).

To further explore the early-stage prognostic value of these survival-related genes, we conducted OS analysis on the six prognostic genes only in patients of stage I and II. The results showed that high expression of KIF15 and BUB1B could predict shorter overall survival time compared to patients with low expression in the early stage of OC ($P<0.05$) (**Figure 2G**, **2I**). Although the sample sizes of stage I and II patients are quite small, it still provides evidence that KIF15 and BUB1B appear to have a differential expression among patients in early stages, suggesting an effect of the two genes on prognosis beginning at the early stages. Thus, the differential expression among stages of the two genes was analyzed by GEPIA (**Figure 2H**, **2J**). To resolve the lack of samples of Stage I, we use Stage II to represent the early stage in the analysis. The results certificated that KIF15 and BUB1B began to be overexpressed in early stages, at which the expression of both genes was even higher than that of later stages (stage III and IV). Significantly higher expression in early stages could provide possibilities for the genes to help to apply early diagnosis and to be a target of early-stage therapeutic intervention. However, the expression level of BUB1B in OC tissue had been experimentally verified on 50 Chinese patients by immunohistochemistry in a previous study [10] while KIF15 had not been reported experimentally analyzed both on expression level and cell function. Moreover, the *F* value revealed that the KIF15 (F value = 5.03) had a greater expressional difference among stages than that of BUB1B (F value = 4.7). Therefore, KIF15 was first selected to be expressionally and functionally validated.

As a possible histopathologic biomarker, KIF15 was also compared with KI67, the most commonly used proliferation-associated biomarker, from a bioinformatic perspective. We found that KI67 (the encoded protein of gene MKI67)

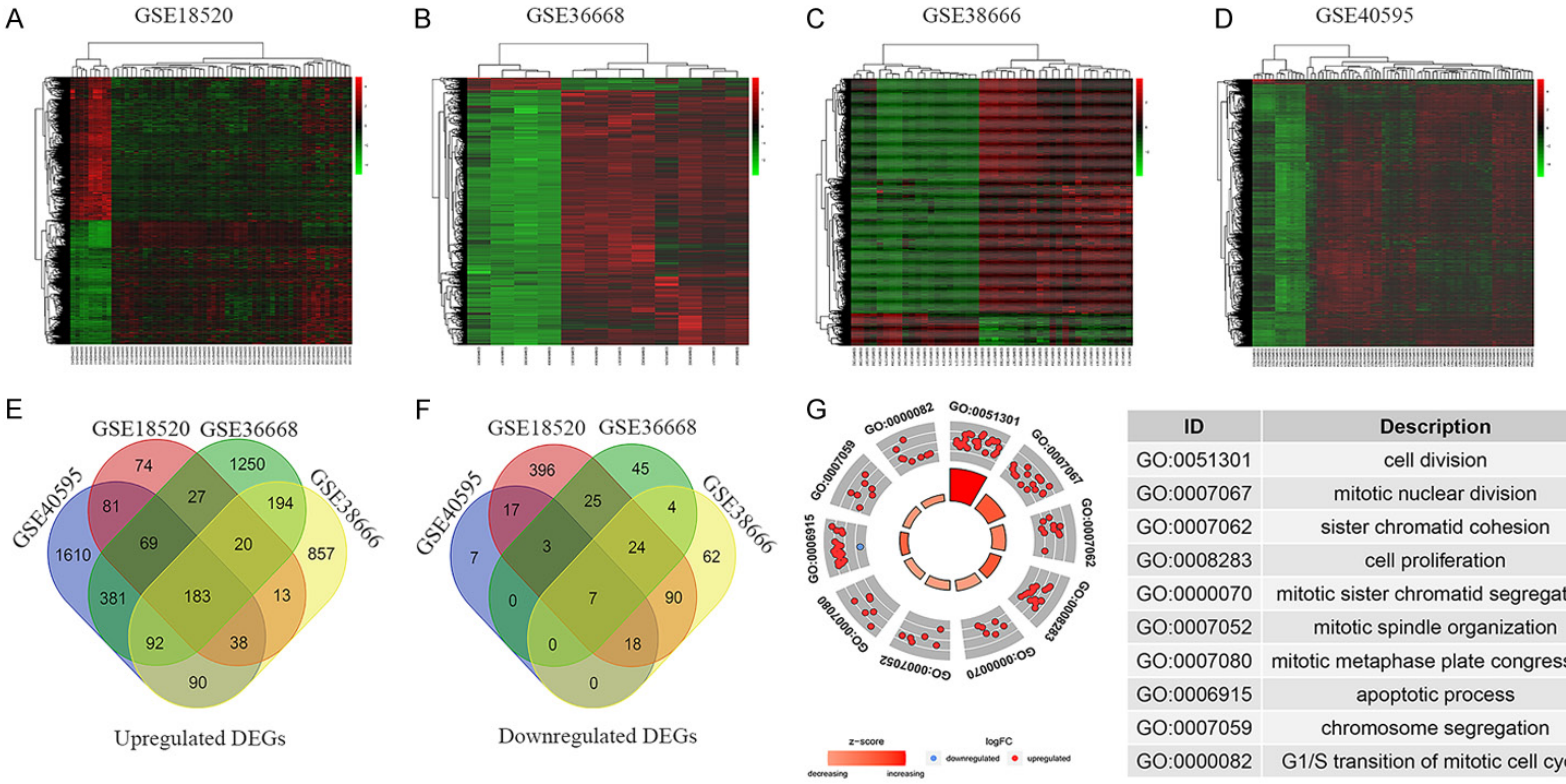

ID	Description
GO:0051301	cell division
GO:0007067	mitotic nuclear division
GO:0007062	sister chromatid cohesion
GO:0008283	cell proliferation
GO:0000070	mitotic sister chromatid segregation
GO:0007052	mitotic spindle organization
GO:0007080	mitotic metaphase plate congression
GO:0006915	apoptotic process
GO:0007059	chromosome segregation
GO:0000082	G1/S transition of mitotic cell cycle

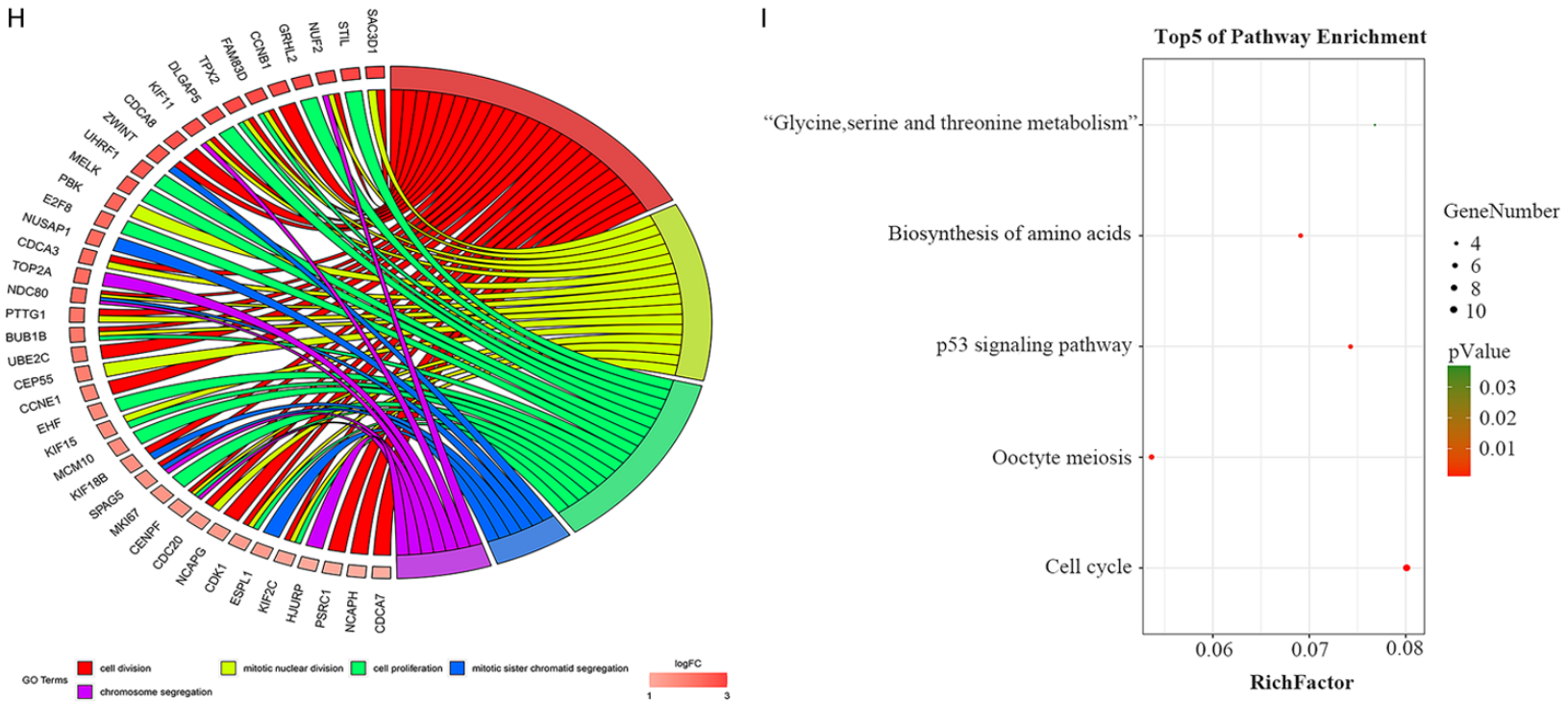

Figure 1. Identification of differentially expressed genes (DEGs) from four GEO datasets of ovarian cancer (OC) and functional and pathway enrichment analysis of consistent DEGs of the datasets. A-D. Heatmaps of DEGs from four datasets of gene expression profiling. E, F. Overlapped part of upregulated and downregulated DEGs in four OC datasets. G. Ten GO categories with the smallest *p*-value. H. Genes in five proliferation-associated BP categories. I. KEGG pathway analysis of the overlapped part of the DEGs from four GEO datasets.

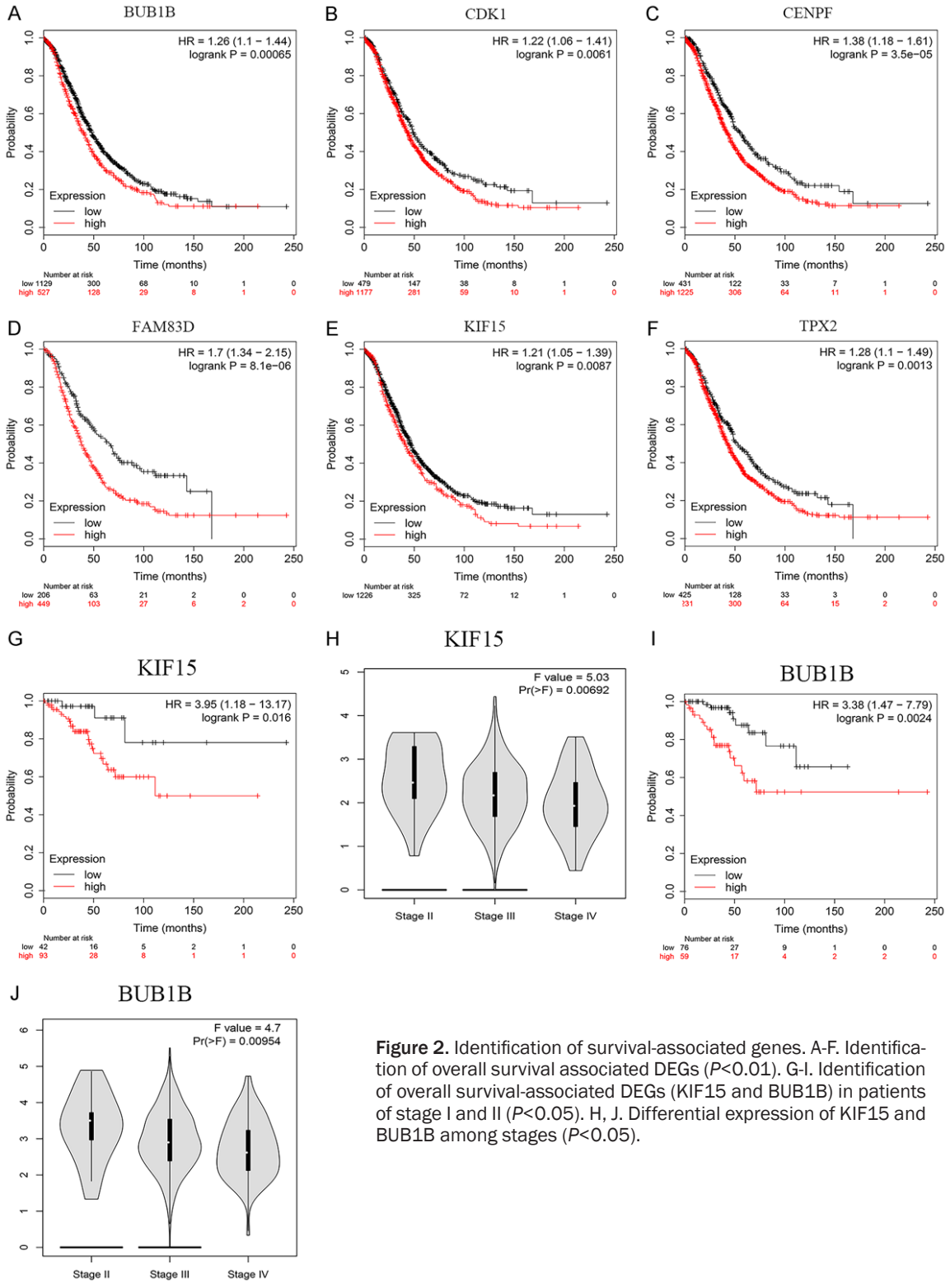

Figure 2. Identification of survival-associated genes. A-F. Identification of overall survival associated DEGs (*P*<0.01). G-I. Identification of overall survival-associated DEGs (KIF15 and BUB1B) in patients of stage I and II (*P*<0.05). H, J. Differential expression of KIF15 and BUB1B among stages (*P*<0.05).

was not significantly associated with the OS rate of OC patients but had early-prognostic value in OC patients of stage I and II (P=0.014, Figure S2A, S2B). However, compared to KIF15, KI67 had no significant expressional difference between earlier and later stages (Figure S2C),

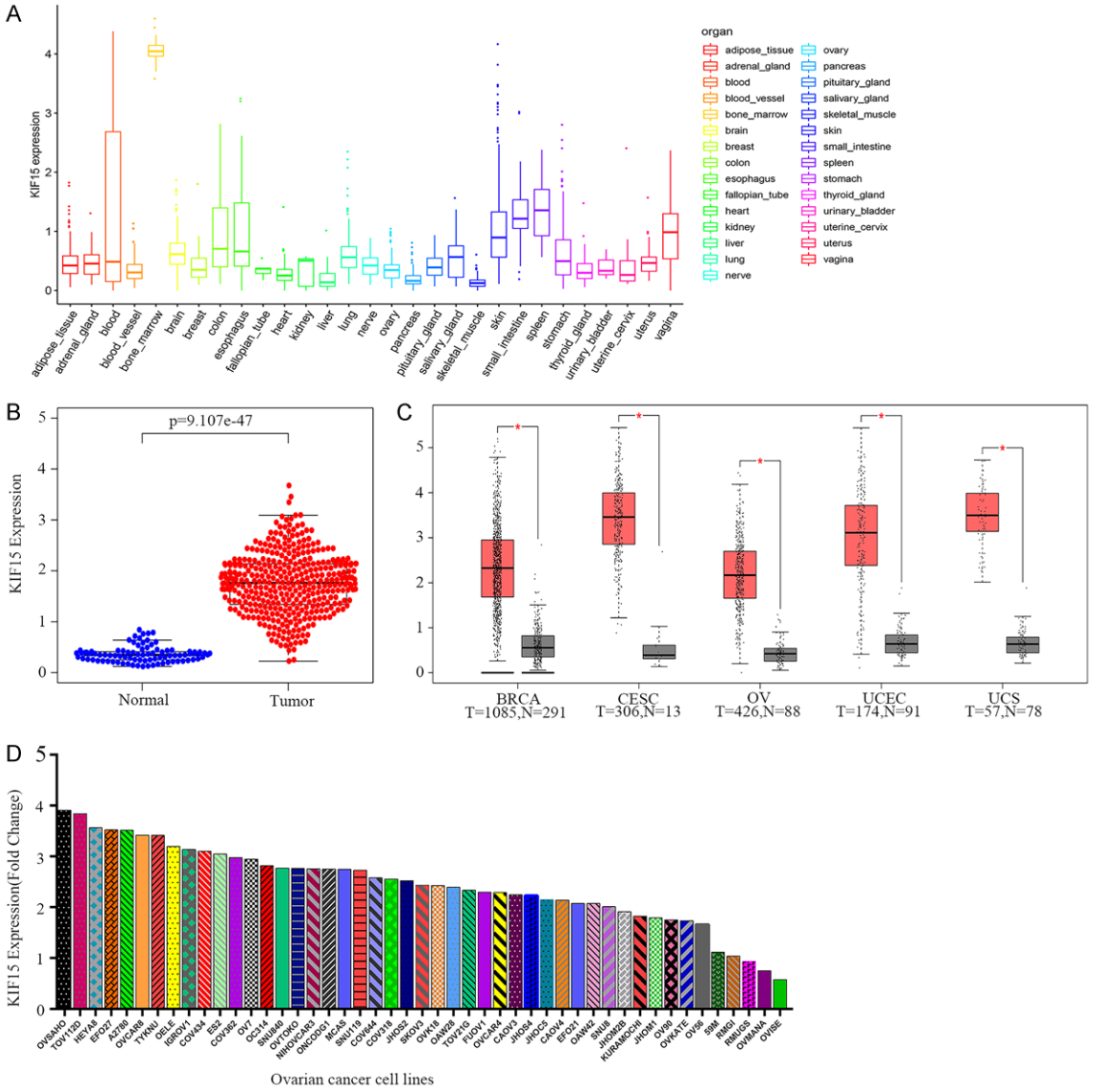

Figure 3. KIF15 expression in tissues and ovarian cancer cell lines by bioinformatic analysis. A. KIF15 expression level in multiple normal tissues of females. B. Comparison of KIF15 expression level between normal ovarian tissue and ovarian cancer samples ($P<0.05$). C. KIF15 overexpression in five female-specific malignancies (Red boxplots represent ovarian cancer samples, gray boxplots represent normal ovarian tissues. *$P<0.05$). D. KIF15 expression in ovarian cancer cell lines.

indicating a lower possibility contributing to early detection and prognosis. Moreover, the expressional correlation between KIF15 and MKI67 was analyzed and the results showed a close correlation (R=0.82, P=4.3e-128, Figure S2D) between the two genes.

KIF15 expression level studied in multiple tissues by bioinformatic methods

The KIF15 expression data in multiple normal tissues of females were obtained from the GTEx datasets and visualized (**Figure 3A**). In females, KIF15 has a low expression in major kinds of normal tissues except the bone marrow. To validate the overexpression of KIF15 in OC tissue, the KIF15 expression levels of normal ovary samples from GTEx and OC samples from TCGA were compared. The KIF15 expression of OC samples was significantly higher than in normal ovarian samples (**Figure 3B**), consistent with the results of an analysis of the selected GEO datasets. To further verify the KIF15 overexpression in OC and explore the

expression level in other female-specific malignancies, GEPIA online tools were used to conduct the analysis. We also found that except for the previously certified ovarian cancer, KIF15 was also significantly overexpressed in breast invasive carcinoma (BRCA), cervical squamous cell carcinoma, and endocervical adenocarcinoma (CESC), uterine corpus endometrial carcinoma (UCEC), and uterine carcinosarcoma (UCS) (**Figure 3C**). To preliminarily confirm the feasibility of functional experiments on cell lines, the RNA-seq data of ovarian cell lines from CCLE were downloaded. They showed that KIF15 mRNA was overexpressed in 36/47 ovarian cancer cell lines in CCLE (**Figure 3D**), supporting the feasibility of functional verification on the cellular level.

KIF15 overexpression validated by experimental methods

On a TMA of OC, we also validated the overexpression of KIF15 protein at the tissue level. The samples contained in the online databases such as TCGA are mostly from white patients. Therefore, we used a TMA, in which the samples were all from Asians, to apply in the study to figure out whether the KIF15 expression had a racial difference. In the results of TMA analysis, the KIF15 expression of OC samples was significantly higher than that of the unpaired non-tumor ones (P=0.002, **Figure 4A**, **4B**). The results also suggested that the overexpression of KIF15 in OC tissues might not have an obvious racial difference. We also found that 49/64 OC samples (76.6%) of stage I-II included in the TMA had high expression levels (score 8-12). This was evidence that the upregulation of KIF15 mRNA might originally occur in the early stages of OC and KIF15 and may be a biomarker of early prognosis in OC.

Furthermore, we had validated that ten kinds of cancer cell lines including ovarian cancer (SKOV3, OVCAR3, A2780, and HO8910), cervical cancer (Hela, Siha, and C33a), lung adenocarcinoma (A549), pancreatic cancer (PANC-1), and glioblastoma (U87), all had a high expression of KIF15 mRNA (**Figure 4C**).

Knockdown of KIF15 inhibited proliferation of OC cells in vitro

To illuminate the effect of KIF15 knockdown on cell lines with low and high KIF15 original expression level, SKOV3 and HO8910, with relatively high, and low KIF15 expression among four common OC cell lines were selected to be functionally studied subsequently. The validity of shRNA lentivirus was verified by both RT-PCR and western blot methods (**Figure 5A**, **5B**). According to the results of functional annotation, we first assessed the role of KIF15 in OC cell proliferation. Celligo proliferation assay showed that KIF15 knockdown markedly inhibited the proliferation of both SKOV3 and HO8910 cells (**Figure 5C**, **5D**) and the results were supported by CCK8 assay (**Figure 5E-H**). The results suggested that KIF15 acted as a proliferation-promoting oncogene in OC.

Knockdown of KIF15 promoted apoptosis of OC cells in vitro

To evaluate whether KIF15 may be a therapeutic target of OC, we examined the effect of KIF15 knockdown on cell apoptosis by flow cytometry analysis and Caspase 3/7 assay. The most significant findings were that the knockdown of KIF15 in SKOV3 cells significantly increased the percentage of early apoptotic cells and late apoptotic cells (**Figure 6A-D**). Similar results were also obtained in the HO8910 cell line. The Caspase 3/7 activity in the SKOV3 and HO8910 samples was increased by KIF15 knockdown, indicating that cell apoptosis was activated (**Figure 6E**, **6F**). This shows that targeting KIF15 might be an effective therapeutic strategy in OC.

Knockdown of KIF15 inhibits tumor formation of OC in vivo

To investigate the biologic functions of KIF15 *in vivo*, we selected the relatively high-KIF15 expressed SKOV3 cells to perform experiments *in vivo*. The cells of KIF15-KD and NC group were subcutaneously implanted in the corresponding group of Balb/c nude mice. The volume and weight of each tumor were quantified. Under the imager, the green fluorescence of only one mouse with a tumor was observed in the group of ten mice injected with KIF15-KD cells while it was observed in all mice of NC group, indicating that KIF15 knockdown significantly halted tumor formation *in vivo* (**Figure 7A**, **7B**). The knockdown of KIF15 resulted in a significant decrease in the volume and weight of tumors as well as in the tumor formation ratio (**Figure 7C-E**). IHC analysis of xenograft

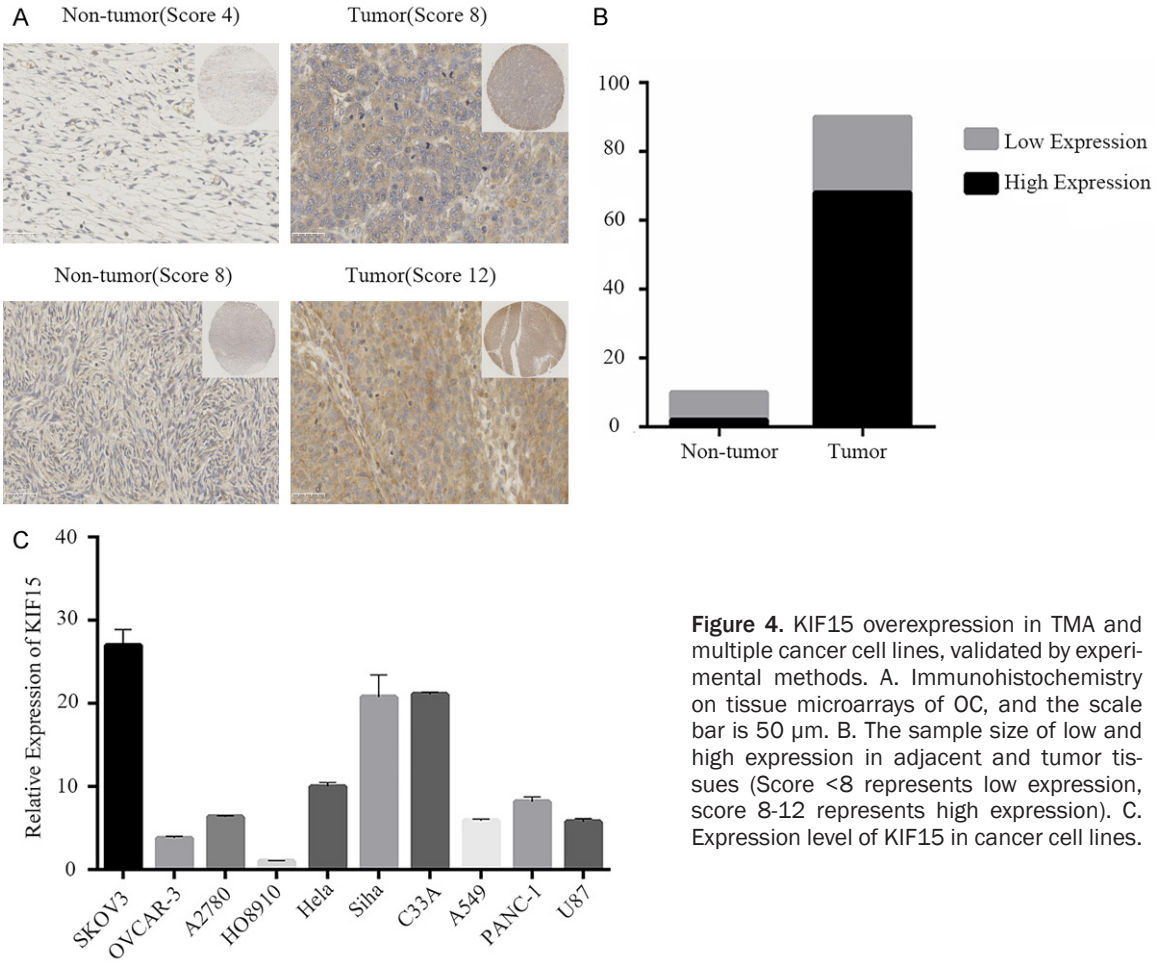

Figure 4. KIF15 overexpression in TMA and multiple cancer cell lines, validated by experimental methods. A. Immunohistochemistry on tissue microarrays of OC, and the scale bar is 50 μm. B. The sample size of low and high expression in adjacent and tumor tissues (Score <8 represents low expression, score 8-12 represents high expression). C. Expression level of KIF15 in cancer cell lines.

tumor tissues also showed that knockdown of KIF15 significantly impeded tumor formation *in vivo* (**Figure 7F**).

KIF15 knockdown promotes OC cell apoptosis by crosstalk among multiple pathways

To further elucidate the mechanisms underlying apoptosis promotion by KIF15 knockdown, KIF15-KD, and NC cell samples were analyzed by mRNA microarray and phospho-antibody arrays. The same samples were used to extract mRNA and proteins to avoid the batch effect. We obtained 134 upregulated and 309 downregulated DEGs from mRNA expression profiling after KIF15 knockdown (**Figure 8A**). In the pathway networks constructed by ClueGO, we found that many key DEGs were enriched for the intrinsic apoptosis pathway, TNF signaling pathway, and NF-kappa B (NF-kB) signaling pathway (**Figure 8B**). Consistently, the results of GSEA analysis showed that apoptosis and TNFα signaling by NFkb were hallmarks of the DEGs (**Figure 8C**).

To further understand the activation of apoptosis-related pathways, including both the pro-apoptotic and anti-apoptotic pathways after KIF15 knockdown in ovarian cancer cells, we conducted a pathway analysis on the phospho-array results. The phosphorylated proteins on the three apoptosis-related pathways were extracted to build a core network of key phosphorylated proteins (**Figure 8D**, **8G**). It was shown that the three pathways have two intersected nodes on mRNA level (Mitogen-Activated Protein Kinase Kinase Kinase 14 [MAP3K14] and Tumor Necrosis Factor [TNF]) and four on protein level (Nuclear Factor Kappa B Subunit 1 [NFkB-p105/p50, Phospho-Ser337], Inhibitor Of Nuclear Factor Kappa B Kinase Subunit Beta [IKK-beta, Phospho-Tyr199], NF-Kappa-B Transcription Factor P65 [NFkB-p65, Phospho-Ser529] and Inhibitor Of Nuclear Factor Kappa

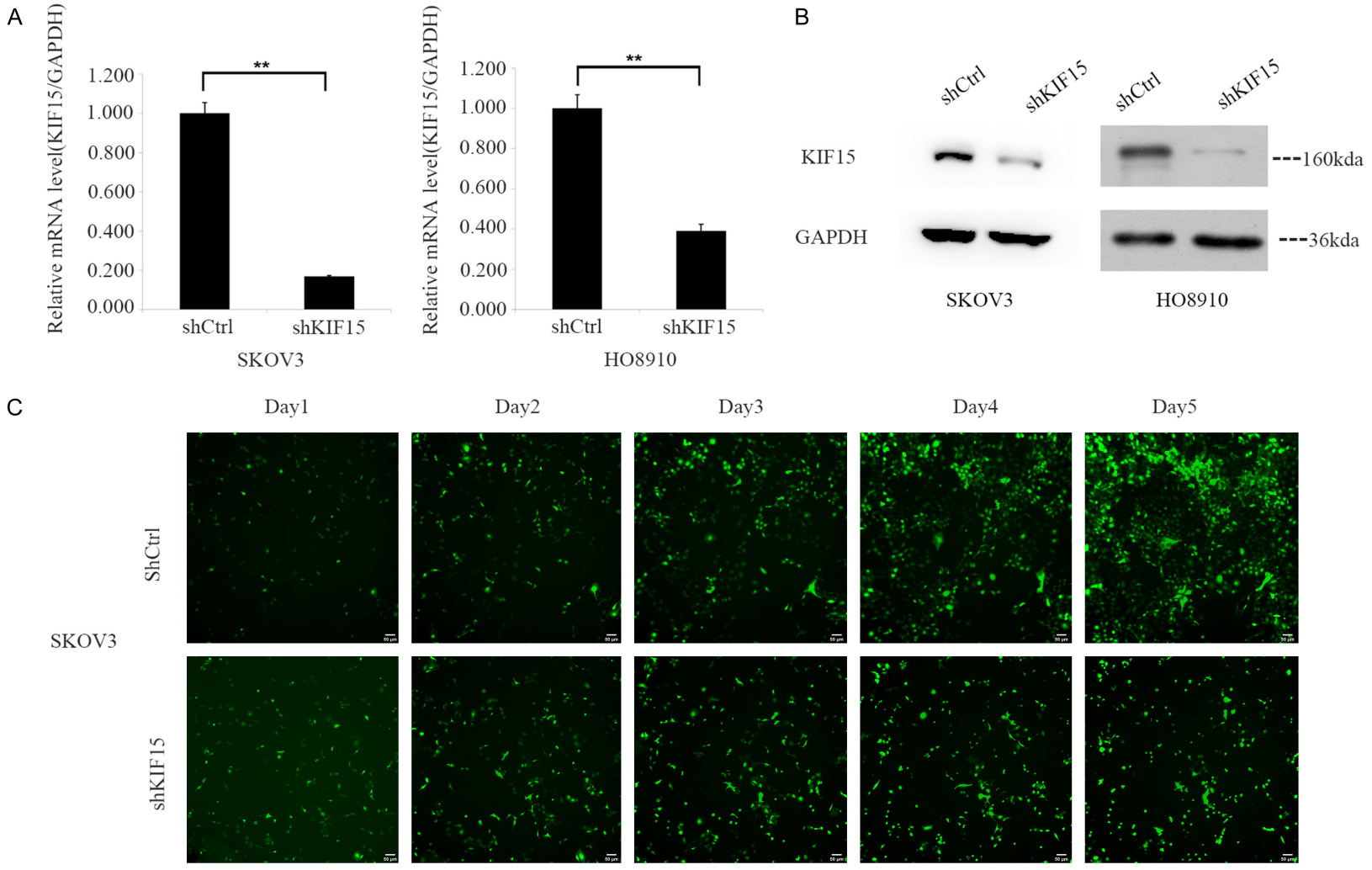
A
Relative mRNA level(KIF15/GAPDH)
1.200
1.000
0.800
0.600
0.400
0.200
0.000
**
shCtrl
shKIF15
SKOV3
Relative mRNA level(KIF15/GAPDH)
1.200
1.000
0.800
0.600
0.400
0.200
0.000
**
shCtrl
shKIF15
HO8910
B
shCtrl
shKIF15
shCtrl
shKIF15
KIF15
---160kda
GAPDH
---36kda
SKOV3
HO8910
C
Day1
Day2
Day3
Day4
Day5
ShCtrl
SKOV3
shKIF15

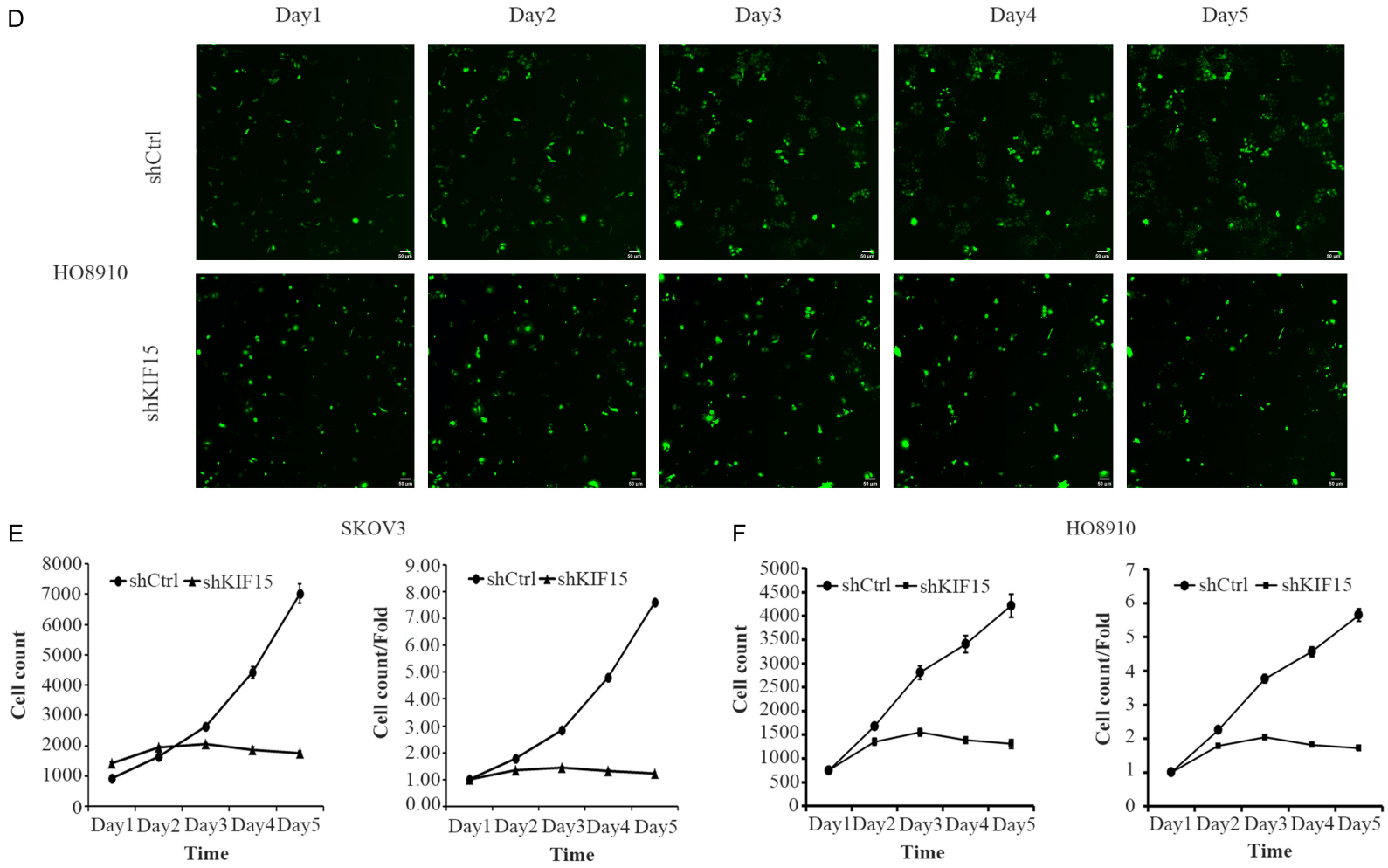
D
Day1
Day2
Day3
Day4
Day5
shCtrl
HO8910
shKIF15
E
SKOV3
shCtrl
shKIF15
Cell count
Time
Cell count/Fold
F
HO8910

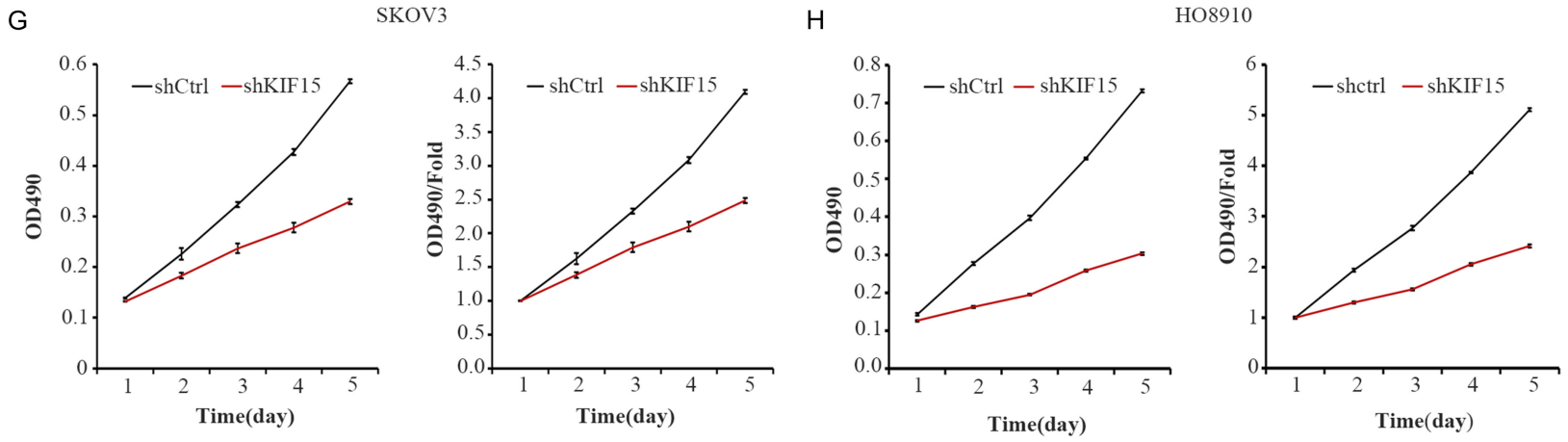

Figure 5. Knockdown of KIF15 inhibits the proliferation of OC cells *in vitro*. A, B. The validity of shRNA lentivirus was verified by RT-PCR (**P<0.01) and western blot. C, D. KIF15 knockdown inhibited SKOV3 and HO8910 proliferation analyzed by the Celigo method, and the scale bar is 50 μm. E, F. Variation trend of cell count and cell count fold change of SKOV3 and HO8910 cell lines. G, H. KIF15 knockdown inhibited SKOV3 and HO8910 proliferation, analyzed by the CCK8 method.

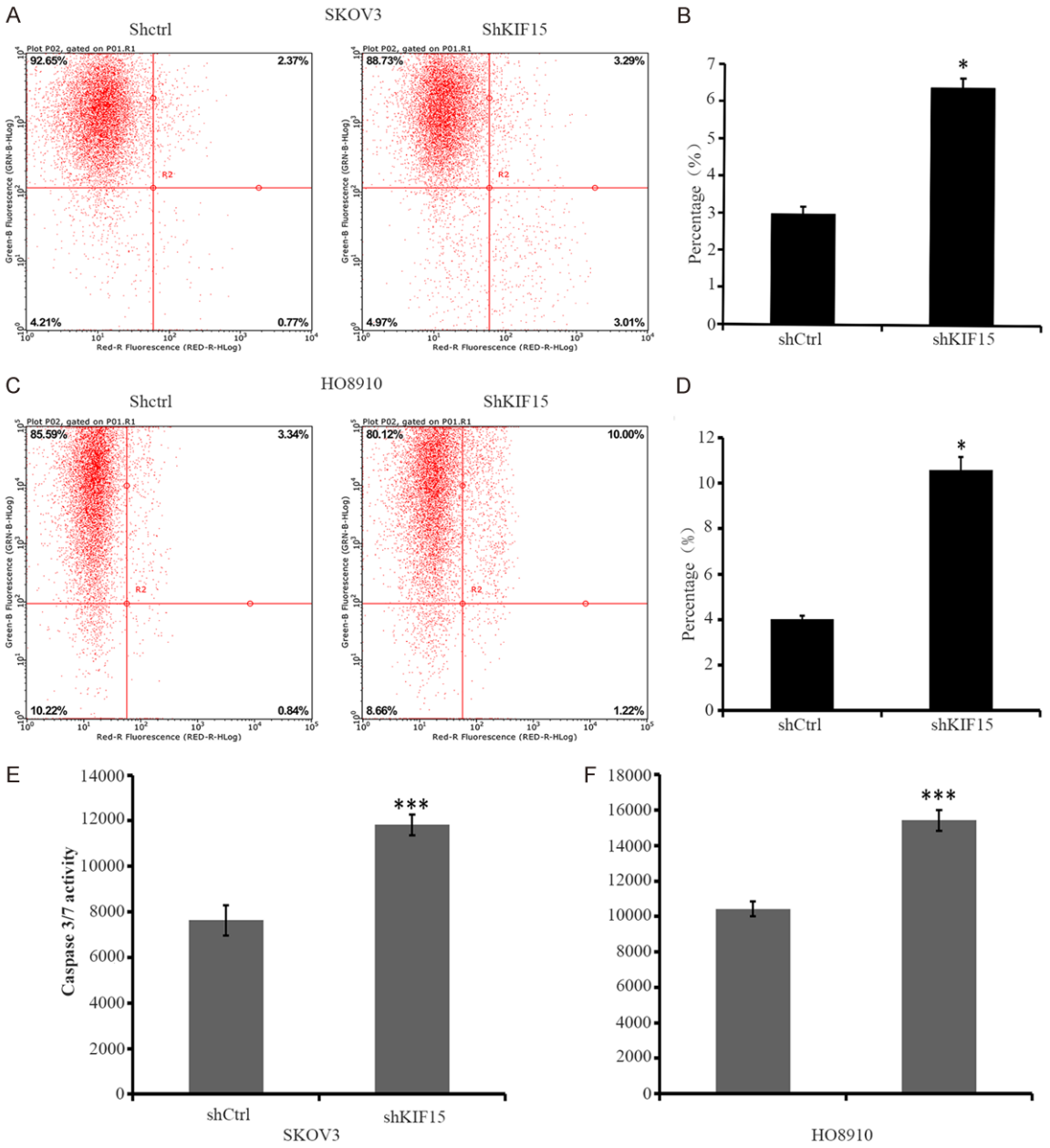

Figure 6. Knockdown of KIF15 promoted apoptosis of OC cells *in vitro*. A-D. Apoptosis of SKOV3 and HO8910 was analyzed by the flow cytometry method. E, F. Apoptosis was analyzed by Caspase 3/7 assay. (**P*<0.05, ****P*<0.001).

B Kinase Regulatory Subunit Gamma [IKK-gamma, Phospho-Ser31]) (**Figure 8E**, **8F**, **8H**). The networks revealed that the significantly phosphorylated proteins AKT Serine/Threonine Kinase 2 (AKT2), Mitogen-Activated Protein Kinase 1 (MAPK1), BCL2 Apoptosis Regulator (BCL-2), BCL2 Associated X Apoptosis Regulator (BAX), BCL2 Associated Agonist Of Cell Death (BAD), and BH3 Interacting Domain Death Agonist (BID) were key proteins among the three pathways (**Figure 8G**). The protein expression change and phosphorylation ratio of the key proteins in **Figure 8G** and **8H** are shown in **Table 1**. A phosphorylation ratio greater than 1.12 was considered significant phosphorylation [26]. The results revealed that all the key nodes had a significantly upregulated phosphorylation level, confirming that crosstalk existed among the three apoptosis-related pathways after KIF15 knockdown.

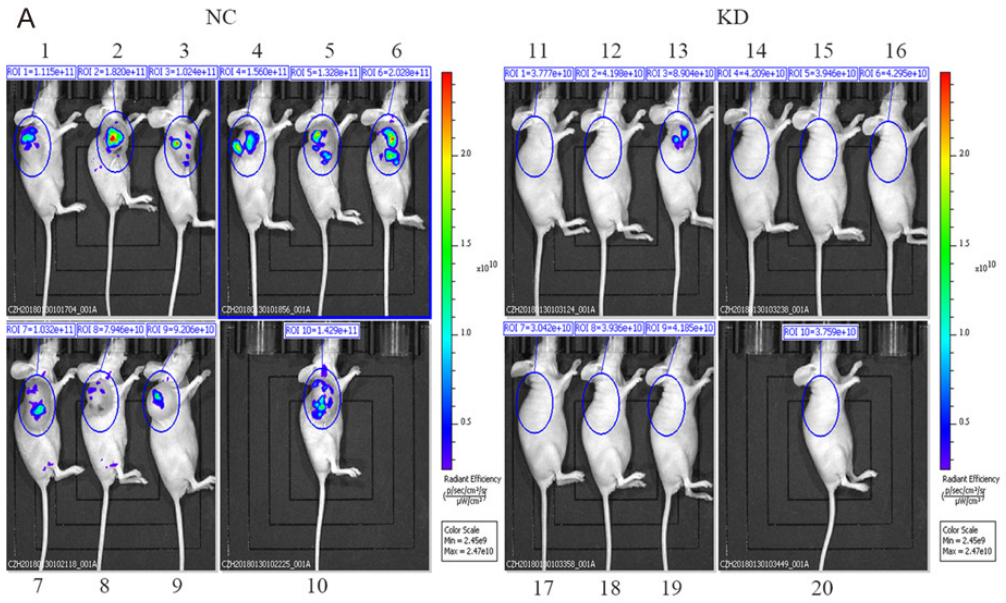
A
NC
KD
1 2 3 4 5 6
11 12 13 14 15 16
7 8 9 10
17 18 19 20
Radiant Efficiency
Color Scale
Min = 2.45e9
Max = 2.47e10

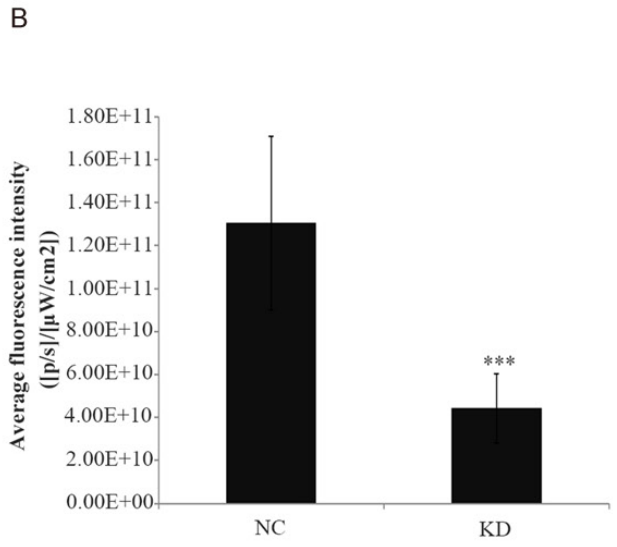
B
Average fluorescence intensity ([p/s]/[μW/cm2])
1.80E+11
1.60E+11
1.40E+11
1.20E+11
1.00E+11
8.00E+10
6.00E+10
4.00E+10
2.00E+10
0.00E+00
***
NC
KD

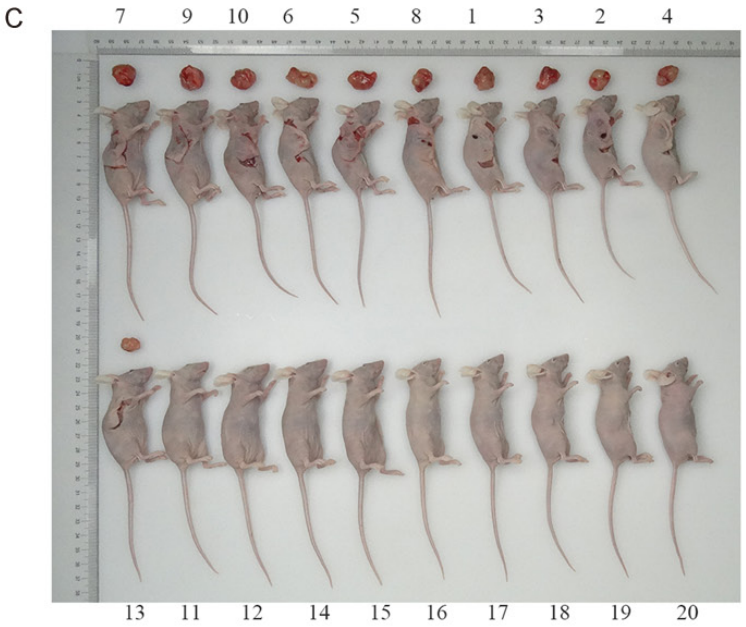
C
7 9 10 6 5 8 1 3 2 4
13 11 12 14 15 16 17 18 19 20

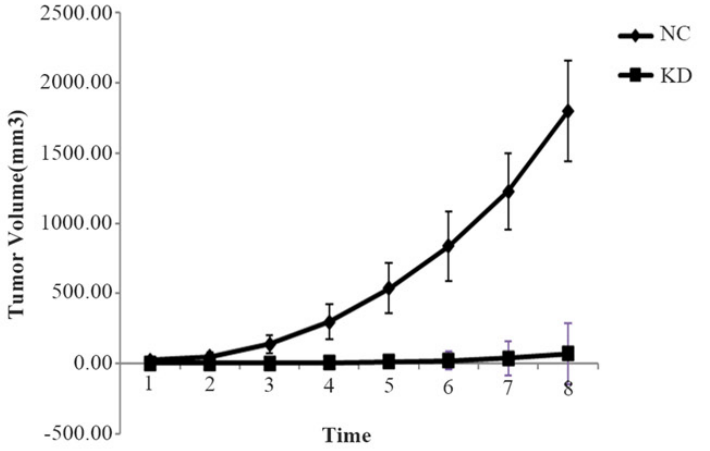
D
Tumor Volume(mm3)
2500.00
2000.00
1500.00
1000.00
500.00
0.00
-500.00
1 2 3 4 5 6 7 8
Time
NC
KD

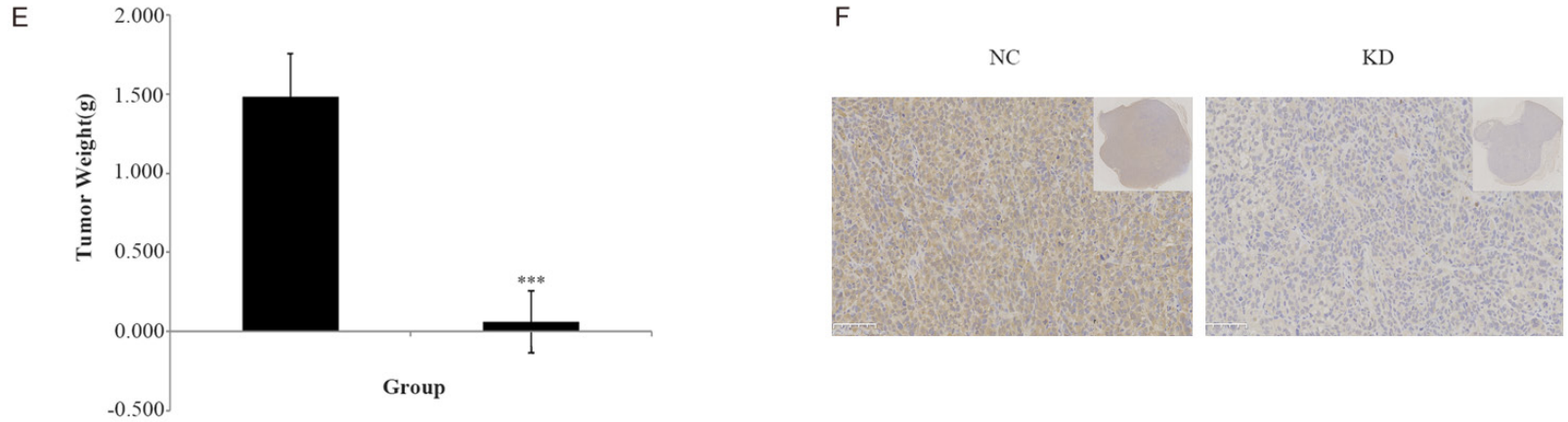

Figure 7. Knockdown of KIF15 inhibited tumor formation of OC *in vivo*. A. Green fluorescence signal of xenograft tumor in mice of NC and KD groups. The mice were numbered 1-10 (NC group), and 11-20 (KD group). B. Average fluorescence intensity of xenograft tumors in mice of NC and KD groups. C. Xenograft tumors and mice of NC and KD groups. D. Variation trend of average tumor volume in NC, and KD groups. E. Average tumor weight of NC and KD groups. F. KIF15 expression in xenograft tumors of NC and KD groups analyzed by IHC, and the scale bar is 100 μm (***P<0.001).

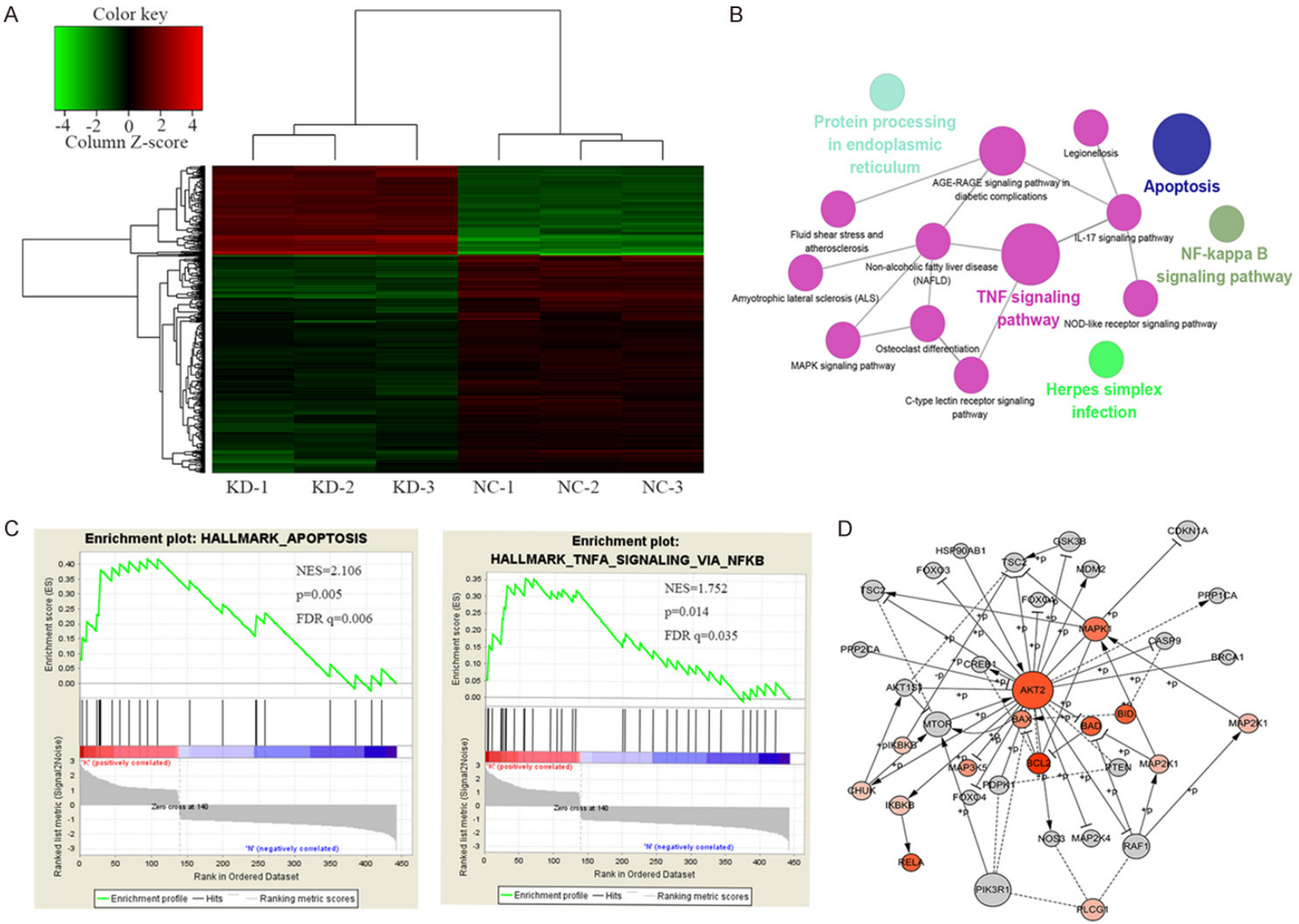
A
Color key
-4 -2 0 2 4
Column Z-score
KD-1
KD-2
KD-3
NC-1
NC-2
NC-3
B
Protein processing in endoplasmic reticulum
AGE-RAGE signaling pathway in diabetic complications
Legionellosis
Apoptosis
Fluid shear stress and atherosclerosis
Non-alcoholic fatty liver disease (NAFLD)
IL-17 signaling pathway
NF-kappa B signaling pathway
Amyotrophic lateral sclerosis (ALS)
TNF signaling pathway
NOD-like receptor signaling pathway
Osteoclast differentiation
MAPK signaling pathway
C-type lectin receptor signaling pathway
Herpes simplex infection
C
Enrichment plot: HALLMARK_APOPTOSIS
NES=2.106
p=0.005
FDR q=0.006
Enrichment score (ES)
Ranked list metric (Signal2Noise)
'A' (positively correlated)
Zero cross at 140
'N' (negatively correlated)
Rank in Ordered Dataset
Enrichment profile
Hits
Ranking metric scores
Enrichment plot:
HALLMARK_TNFA_SIGNALING_VIA_NFKB
NES=1.752
p=0.014
FDR q=0.035
D
HSP90AB1
GSK3B
CDKN1A
FOXO3
TSC2
MDM2
PPP1CA
PPP2CA
CASP9
BRCA1
AKT1S1
AKT2
BAX
BID
MTOR
BAD
MAP2K1
IKBKB
BCL2
PTEN
MAP3K5
PDPK1
CHUK
FOXO4
IKBKB
NOS3
MAP2K4
RAF1
RELA
PIK3R1
PLCG1

E

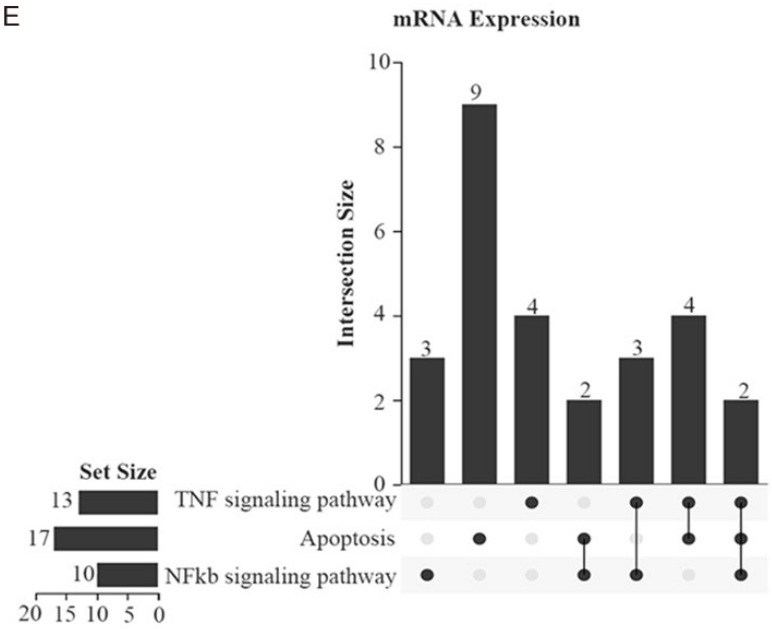
mRNA Expression
Intersection Size
10
8
6
4
2
0
9
4
3
2
3
4
2
Set Size
13
17
10
TNF signaling pathway
Apoptosis
NFkb signaling pathway
20 15 10 5 0

F

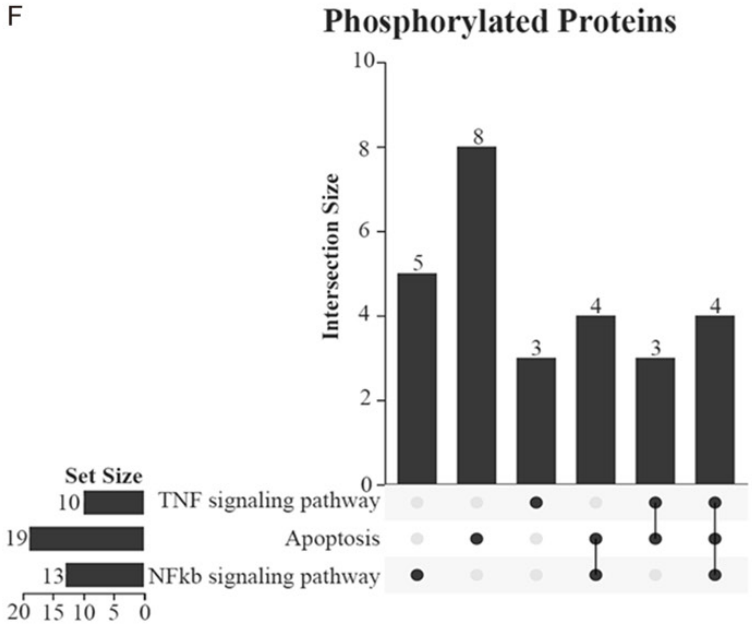
Phosphorylated Proteins
Intersection Size
10
8
6
4
2
0
5
8
3
4
3
4
Set Size
10
19
13
TNF signaling pathway
Apoptosis
NFkb signaling pathway
20 15 10 5 0

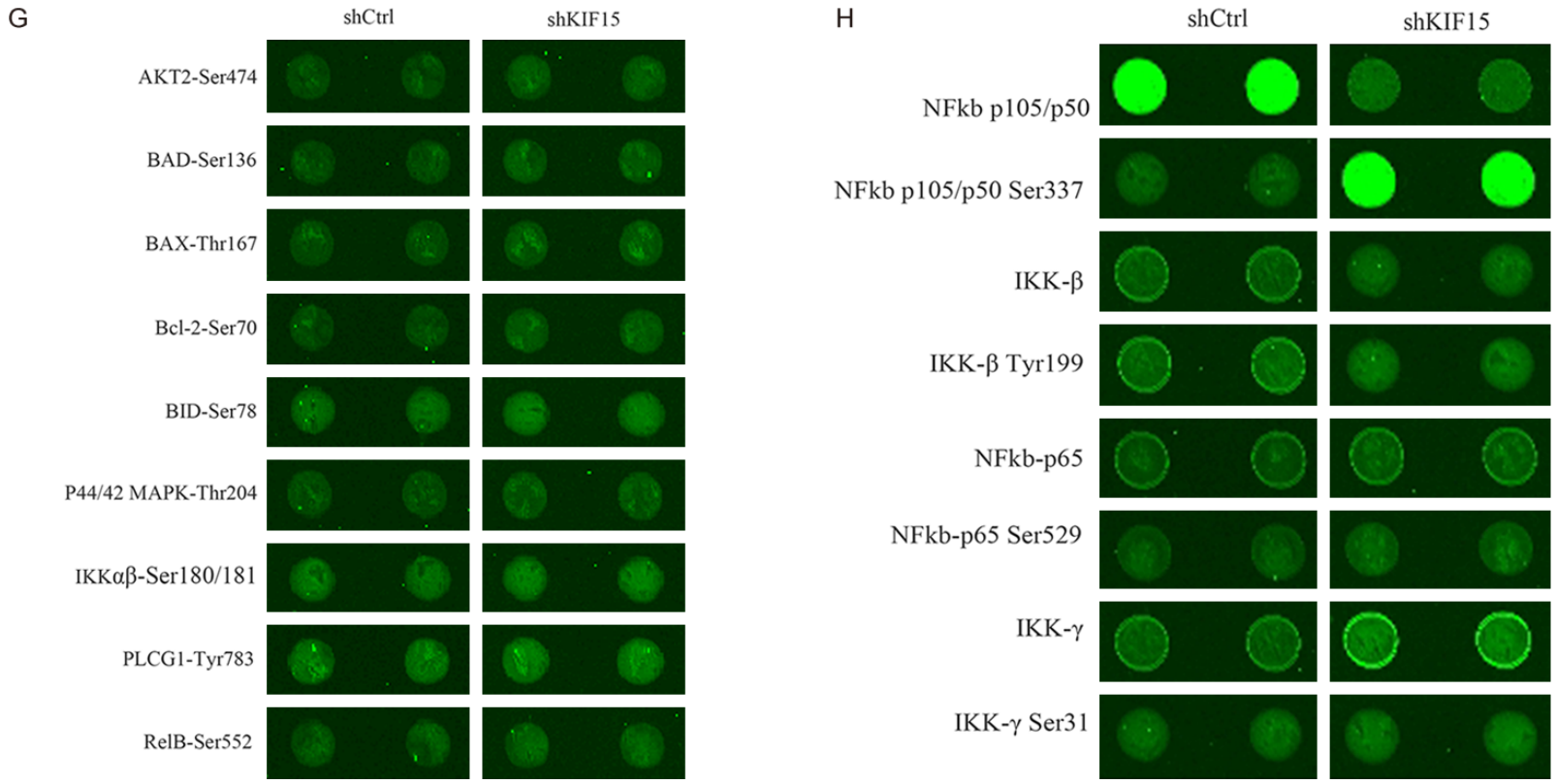

Figure 8. KIF15 knockdown promotes OC cell apoptosis by crosstalk between multiple pathways. A. Heatmap of DEGs obtained from the gene expression profiling after KIF15 knockdown. B. Pathway networks were constructed among the DEGs. C. The hallmarks of the DEGs were analyzed by GSEA. D. The core networks of the key phosphorylated proteins among three apoptosis-related pathways. E, F. Common nodes of three apoptosis-related pathways in mRNA and phosphorylated protein levels. G. Significantly phosphorylated proteins in the core networks. H. Protein and phosphorylated protein expression levels of the four intersected nodes in the three apoptosis-related pathways at the protein level.

Table 1. Fold change of key proteins in the crosstalk of apoptosis-associated pathways

Key Protein	Ratio (KD vs. NC)
AKT2	1.15
AKT2 (Phospho-Ser474)	1.30
BAD (Phospho-Ser136)	1.29
BAX	1.02
BAX (Phospho-Thr167)	1.25
BCL-2 (Phospho-Ser70)	1.33
BID	1.05
BID (Phospho-Ser78)	1.29
p44/42 MAP Kinase	1.19
p44/42 MAP Kinase (Phospho-Tyr204)	1.27
IKKα/β	1.15
IKKα/β (Phospho-Ser180/181)	1.20
PLCG1	1.25
PLCG1 (Phospho-Tyr783)	1.21
RelB	1.20
RelB (Phospho-Ser552)	1.24
NFkB-p105/p50	0.98
NFkB-p105/p50 (Phospho-Ser337)	1.15
IKK-β	1.21
IKK-β (Phospho-Tyr199)	1.18
NFkB-p65	1.25
NFkB-p65 (Phospho-Ser529)	1.29
IKK-γ	1.13
IKK-γ (Phospho-Ser31)	1.15

Discussion

The mortality rate of OC ranks first among gynecologic malignant tumors. Because of its highly asymptomatic nature and lack of reliable biomarkers, advanced-stage diagnosis and the delayed treatment are the main causes of the high mortality of OC. Investigation of novel and reliable biomarkers with early prognostic value could facilitate diagnosis and treatment in the early stages of OC. Uncontrolled proliferation is a crucial feature of malignancies and also an important part of cancer development and progression. Inhibiting sustained proliferation in cancer could be an effective strategy fo target therapies [6]. Here, we used bioinformatics me thods to screen the key genes modulating cell proliferation and having a significant impact on the survival time of patients and performed further experimental research.

In the study, 180 overlapped DEGs were obtained, based on four datasets of gene expression profiling from GEO. By performing GO analysis, we found that in the top 10 GO categories with the lowest *p*-value, five were correlated to the process of cell mitosis and proliferation. From the five GO categories, we obtained 40 proliferation-related genes, in which 17 genes participated in two or more proliferation-related biological processes. This strongly supported that the 17 genes are important nodes on the crossroads of the regulatory network modulating the cell function of proliferation. The survival analysis revealed that 6 in the 17 proliferation-related genes had significant prognostic value, including BUB1B, CDK1, CENPF, FAM83D, KIF15, and TPX2. Studies had reported that upregulation of BUB1B, KIF15 [8], CDK1 [27], CENPF [28], FAM83D [29], and *TPX2* [30] all predicted poor prognosis in OC. However, whether these survival-associated genes have early prognostic value in patients of stage I-II has not been reported.

To explore the early prognostic value of these genes, we conducted overall survival analysis on patients of stage I and II and found that the upregulation of BUB1B and KIF15 in early stages could predict poor prognosis of OC patients. It also indicated that these two genes began to be overexpressed and played crucial roles to impact the prognosis of patients in the early stages. Therefore, BUB1B and KIF15 might be prognostic indicators, pathologic diagnostic biomarkers, and therapeutic targets in early stages in OC. By using GEPIA online tool, we discovered that both KIF15 and BUB1B had a significant expressional difference between earlier stages (stage II) and later stages (stage III-IV). The biomarkers with significantly higher expression in early stages might provide a possibility for early diagnosis and targeted therapies in the early stages. However, BUB1B had been bioinformatically analyzed and expressionally verified on OC tissues in a previous study while KIF15 had not been reported bioinformatically and experimentally analyzed in OC. Also taking the *F* value and *p* value into consideration, KIF15 was first selected as the candidate gene to be experimentally studied while BUB1B still needed to be functionally analyzed in our following work.

As a candidate proliferation-associated biomarker, KIF15 was also compared to KI67, a clinically commonly used histopathologic biomarker. By using bioinformatic methods, we found that the mRNA expression of KIF15 and

MKI67 had a correlation coefficient over 0.8 which suggests co-expression of the two genes and provided some evidence that KIF15 could be a proliferation-associated histopathologic biomarker similar to KI67. However, the bioinformatic analysis was conducted only on the mRNA level. To validate whether KIF15 could be a widely-used histopathologic biomarker, a large validation study on OC is still needed.

KIF15 is a member of the kinesin superfamily and a microtubule-associated protein that participates in the mitotic process. Although the structure and molecular functions of KIF15 have been studied for approximately 10 years, the role of KIF15 in the tumorigenesis and progression of OC has not yet been illuminated. A previous study had reported that KIF15 promoted the proliferation of cancer cells in pancreatic cancer [31], bladder cancer [32], breast cancer [33], and osteosarcoma [34]. This indicates that KIF15 is a proliferation-related biomarker in multiple malignancies, similar to our findings with ovarian cancer in this study.

The proliferation of cancer cells is an important target of anti-tumor therapeutic strategies. In our study, we found that targeting KIF15 promoted apoptosis of OC cancer cells, highlighting the potential of KIF15 as a therapeutic target to slow down the tumor growth and further delay the progression of OC. Otherwise, we also found that KIF15 was overexpressed in five kinds of female-specific cancer but had low expression levels in the corresponding normal tissues. This suggested KIF15 had the potential to be a consistent therapeutic target of female malignancies and simultaneously avoid an off-target effect.

Recent studies had reported that KIF15 was a hub gene associated with cancer stem cell proliferation in lung squamous cell carcinoma [35] by the bioinformatic method of Weighted Gene Co-Expression Network Analysis (WGCNA). Otherwise, KIF15 was also experimentally proven to promote cancer stem cell phenotype and malignancy in hepatocellular carcinoma [36]. These results indicated that KIF15 was not only a target of anti-proliferation therapies in cancers but also a possible target of anti-CSC therapies. However, whether KIF15 plays a CSC-related role in OC and whether the early prognosis value of KIF15 is associated with the stemness maintenance of stem cells from the initial tumor, are still unclear and waiting for further research.

In the present study, the crosstalk of three apoptosis-associated pathways after KIF15 knockdown was discovered by gene expression profiling, and the activation was proven by phospho-antibody arrays. Interestingly, we found that both pro-apoptotic and anti-apoptotic pathways were activated and crosstalked with each other. The intrinsic apoptotic pathway is a vital pro-apoptotic pathway in the apoptotic process of ovarian cancer [37]. However, researchers have reported that NFkb activation could suppress the TNFα-induced apoptosis of cells [38]. By analyzing the result of phospho-antibody arrays, we found that the TNF signaling pathway was activated. The expression of *RELA* (NFkb-p65), a subunit of NFkb, was upregulated and the protein was significantly phosphorylated, indicating an obvious activation. Moreover, the hub gene AKT2 in the core network, which was upregulated and phosphorylated, plays an anti-apoptosis role in ovarian cancer [39]. We also found that the anti-apoptotic protein BCL-2 was significantly phosphorylated and BCLXL was mildly phosphorylated and expressionally upregulated. Otherwise, the pro-apoptotic proteins BAX, BAD, and BID were all significantly activated. The results illuminated that after KIF15 knockdown, the mechanisms of anti-apoptosis and pro-apoptosis coexisted. However, according to our research, it showed a pro-apoptotic effect eventually. A recent study had reported that knockdown of KIF15 promoted apoptosis in cancer cells, but whether anti-apoptosis mechanisms existed was unclear [34]. If the anti-apoptosis after KIF15 knockdown is a self-protection mechanism to resist cell death, it strongly supports KIF15 as an important regulator of cell survival.

Conclusion

KIF15 is a proliferation-related biomarker with early prognostic and histopathologic diagnostic value in OC. Targeting KIF15 inhibited tumor formation and growth through restraining proliferation and promoting apoptosis of OC cells. The promoted apoptosis of OC cells was regulated by the network constructed by both pro-apoptotic pathways and anti-apoptotic pathways. Therefore, KIF15 may also be a therapeutic target in OC.

Acknowledgements

This work was supported by the National Key Technology R&D Program of China (No.2019YFC1005202 and 2019YFC1005204) and the Clinical Innovation Foundation of Southwest Hospital of China (No. SWH2016ZDCX1013).

Disclosure of conflict of interest

None.

Address correspondence to: Zhiqing Liang, Department of Gynecology and Obstetrics, Southwest Hospital, Army Medical University, No. 30 Gaotanyan Street, Shapingba District, Chongqing 400038, China. ORCID: https://orcid.org/0000-0002-8608-2857; E-mail: zhiqingliang2020@163.com

References

[1] Torre LA, Trabert B, DeSantis CE, Miller KD, Samimi G, Runowicz CD, Gaudet MM, Jemal A and Siegel RL. Ovarian cancer statistics, 2018. CA Cancer J Clin 2018; 68: 284-296.

[2] Xi QP, Pu DH and Lu WN. Research on application value of combined detection of serum CA125, HE4 and TK1 in the diagnosis of ovarian cancer. Eur Rev Med Pharmacol Sci 2017; 21: 4536-4541.

[3] Dizon DS. PARP inhibitors for targeted treatment in ovarian cancer. Lancet 2017; 390: 1929-1930.

[4] Edgar R, Domrachev M and Lash AE. Gene expression omnibus: NCBI gene expression and hybridization array data repository. Nucleic Acids Res 2002; 30: 207-210.

[5] Cancer Genome Atlas Research Network, Weinstein JN, Collisson EA, Mills GB, Shaw KR, Ozenberger BA, Ellrott K, Shmulevich I, Sander C and Stuart JM. The Cancer Genome Atlas Pan-Cancer analysis project. Nat Genet 2013; 45: 1113-1120.

[6] Feitelson MA, Arzumanyan A, Kulathinal RJ, Blain SW, Holcombe RF, Mahajna J, Marino M, Martinez-Chantar ML, Nawroth R, Sanchez-Garcia I, Sharma D, Saxena NK, Singh N, Vlachostergios PJ, Guo S, Honoki K, Fujii H, Georgakilas AG, Bilsland A, Amedei A, Niccolai E, Amin A, Ashraf SS, Boosani CS, Guha G, Ciriolo MR, Aquilano K, Chen S, Mohammed SI, Azmi AS, Bhakta D, Halicka D, Keith WN and Nowsheen S. Sustained proliferation in cancer: Mechanisms and novel therapeutic targets. Semin Cancer Biol 2015; 35 Suppl: S25-S54.

[7] Yang X, Zhu S, Li L, Zhang L, Xian S, Wang Y and Cheng Y. Identification of differentially expressed genes and signaling pathways in ovarian cancer by integrated bioinformatics analysis. Onco Targets Ther 2018; 11: 1457-1474.

[8] Feng H, Gu ZY, Li Q, Liu QH, Yang XY and Zhang JJ. Identification of significant genes with poor prognosis in ovarian cancer via bioinformatical analysis. J Ovarian Res 2019; 12: 35.

[9] Shen J, Yu S, Sun X, Yin M, Fei J and Zhou J. Identification of key biomarkers associated with development and prognosis in patients with ovarian carcinoma: evidence from bioinformatic analysis. J Ovarian Res 2019; 12: 110.

[10] Zhang L, Sun L, Zhang B and Chen L. Identification of differentially expressed genes (degs) relevant to prognosis of ovarian cancer by use of integrated bioinformatics analysis and validation by immunohistochemistry assay. Med Sci Monit 2019; 25: 9902-9912.

[11] Fekete JT, Ősz Á, Pete I, Nagy GR, Vereczkey I and Győrffy B. Predictive biomarkers of platinum and taxane resistance using the transcriptomic data of 1816 ovarian cancer patients. Gynecol Oncol 2020; 156: 654-661.

[12] Yeung TL, Leung CS, Wong KK, Samimi G, Thompson MS, Liu J, Zaid TM, Ghosh S, Birrer MJ and Mok SC. TGF-β modulates ovarian cancer invasion by upregulating CAF-derived versican in the tumor microenvironment. Cancer Res 2013; 73: 5016-5028.

[13] Mok SC, Bonome T, Vathipadiekal V, Bell A, Johnson ME, Wong KK, Park DC, Hao K, Yip DKP, Donninger H, Ozbun L, Samimi G, Brady J, Randonovich M, Pise-Masison CA, Barrett JC, Wong WH, Welch WR, Berkowitz RS and Birrer MJ. A gene signature predictive for outcome in advanced ovarian cancer identifies a survival factor: microfibril-associated glycoprotein 2. Cancer cell 2009; 16: 521-532.

[14] Lili LN, Matyunina LV, Walker LD, Benigno BB and McDonald JF. Molecular profiling predicts the existence of two functionally distinct classes of ovarian cancer stroma. Biomed Res Int 2013; 2013: 846387.

[15] Elgaaen BV, Olstad OK, Sandvik L, Odegaard E, Sauer T, Staff AC and Gautvik KM. ZNF385B and VEGFA are strongly differentially expressed in serous ovarian carcinomas and correlate with survival. PLoS One 2012; 7: e46317.

[16] Heber S and Sick B. Quality assessment of Affymetrix GeneChip data. OMICS 2006; 10: 358-368.

[17] Ritchie ME, Phipson B, Wu D, Hu Y, Law CW, Shi W and Smyth GK. limma powers differential expression analyses for RNA-sequencing and microarray studies. Nucleic Acids Res 2015; 43: e47.

[18] Huang da W, Sherman BT and Lempicki RA. Bioinformatics enrichment tools: paths toward

the comprehensive functional analysis of large gene lists. Nucleic Acids Res 2009; 37: 1-13.
[19] Walter W, Sánchez-Cabo F and Ricote M. GOplot: an R package for visually combining expression data with functional analysis. Bioinformatics (Oxford, England) 2015; 31: 2912-2914.
[20] Tang Z, Li C, Kang B, Gao G, Li C and Zhang Z. GEPIA: a web server for cancer and normal gene expression profiling and interactive analyses. Nucleic Acids Res 2017; 45: W98-W102.
[21] Cancer Cell Line Encyclopedia Consortium; Genomics of Drug Sensitivity in Cancer Consortium. Pharmacogenomic agreement between two cancer cell line data sets. Nature 2015; 528: 84-87.
[22] Yu X, He X, Heindl LM, Song X, Fan J and Jia R. KIF15 plays a role in promoting the tumorigenicity of melanoma. Exp Eye Res 2019; 185: 107598.
[23] Liu D, Zhang XX, Li MC, Cao CH, Wan DY, Xi BX, Tan JH, Wang J, Yang ZY, Feng XX, Ye F, Chen G, Wu P, Xi L, Wang H, Zhou JF, Feng ZH, Ma D and Gao QL. C/EBPβ enhances platinum resistance of ovarian cancer cells by reprogramming H3K79 methylation. Nat Commun 2018; 9: 1739.
[24] Bindea G, Mlecnik B, Hackl H, Charoentong P, Tosolini M, Kirilovsky A, Fridman WH, Pagès F, Trajanoski Z and Galon J. ClueGO: a Cytoscape plug-in to decipher functionally grouped gene ontology and pathway annotation networks. Bioinformatics (Oxford, England) 2009; 25: 1091-1093.
[25] Liberzon A, Birger C, Thorvaldsdóttir H, Ghandi M, Mesirov JP and Tamayo P. The molecular signatures database (MSigDB) hallmark gene set collection. Cell Syst 2015; 1: 417-425.
[26] Zhang YM, Dai BL, Zheng L, Zhan YZ, Zhang J, Smith WW, Wang XL, Chen YN and He LC. A novel angiogenesis inhibitor impairs lovo cell survival via targeting against human VEGFR and its signaling pathway of phosphorylation. Cell Death Dis 2012; 3: e406.
[27] Xi Q, Huang M, Wang Y, Zhong J, Liu R, Xu G, Jiang L, Wang J, Fang Z and Yang S. The expression of CDK1 is associated with proliferation and can be a prognostic factor in epithelial ovarian cancer. Tumour Biol 2015; 36: 4939-4948.
[28] Xu Z, Zhou Y, Cao Y, Dinh TL, Wan J and Zhao M. Identification of candidate biomarkers and analysis of prognostic values in ovarian cancer by integrated bioinformatics analysis. Med Oncol 2016; 33: 130.
[29] Zhang Q, Yu S, Lok SIS, Wong AST, Jiao Y and Lee LTO. FAM83D promotes ovarian cancer progression and its potential application in diagnosis of invasive ovarian cancer. J Cell Mol Med 2019; 23: 4569-4581.
[30] Cáceres-Gorriti KY, Carmona E, Barrès V, Rahimi K, Létourneau IJ, Tonin PN, Provencher D and Mes-Masson AM. RAN nucleo-cytoplasmic transport and mitotic spindle assembly partners XPO7 and TPX2 are new prognostic biomarkers in serous epithelial ovarian cancer. PLoS One 2014; 9: e91000.
[31] Wang J, Guo X, Xie C and Jiang J. KIF15 promotes pancreatic cancer proliferation via the MEK-ERK signalling pathway. Br J Cancer 2017; 117: 245-255.
[32] Zhao H, Bo Q, Wu Z, Liu Q, Li Y, Zhang N, Guo H and Shi B. KIF15 promotes bladder cancer proliferation via the MEK-ERK signaling pathway. Cancer Manag Res 2019; 11: 1857-1868.
[33] Sheng J, Xue X and Jiang K. Knockdown of kinase family 15 inhibits cancer cell proliferation in vitro and its clinical relevance in triple-negative breast cancer. Curr Mol Med 2019; 19: 147-155.
[34] Wu Z, Zhang H, Sun Z, Wang C, Chen Y, Luo P and Yan W. Knockdown of kinesin family 15 inhibits osteosarcoma through suppressing cell proliferation and promoting cell apoptosis. Chemotherapy 2019; 64: 187-196.
[35] Qin S, Long X, Zhao Q and Zhao W. Co-expression network analysis identified genes associated with cancer stem cell characteristics in lung squamous cell carcinoma. Cancer Invest 2020; 38: 13-22.
[36] Li Q, Qiu J, Yang H, Sun G, Hu Y, Zhu D, Deng Z, Wang X, Tang J and Jiang R. Kinesin family member 15 promotes cancer stem cell phenotype and malignancy via reactive oxygen species imbalance in hepatocellular carcinoma. Cancer Lett 2020; 482: 112-125.
[37] Nordin N, Fadaeinasab M, Mohan S, Mohd Hashim N, Othman R, Karimian H, Iman V, Ramli N, Mohd Ali H and Abdul Majid N. Pulchrin A, a new natural coumarin derivative of enicosanthellum pulchrum, Induces apoptosis in ovarian cancer cells via intrinsic pathway. PLoS One 2016; 11: e0154023.
[38] Van Antwerp DJ, Martin SJ, Kafri T, Green DR and Verma IM. Suppression of TNF-alpha-induced apoptosis by NF-kappaB. Science 1996; 274: 787-789.
[39] Ding Z, Xu F, Li G, Tang J, Tang Z, Jiang P and Wu H. Knockdown of Akt2 expression by shRNA inhibits proliferation, enhances apoptosis, and increases chemosensitivity to paclitaxel in human colorectal cancer cells. Cell Biochem Biophys 2015; 71: 383-388.

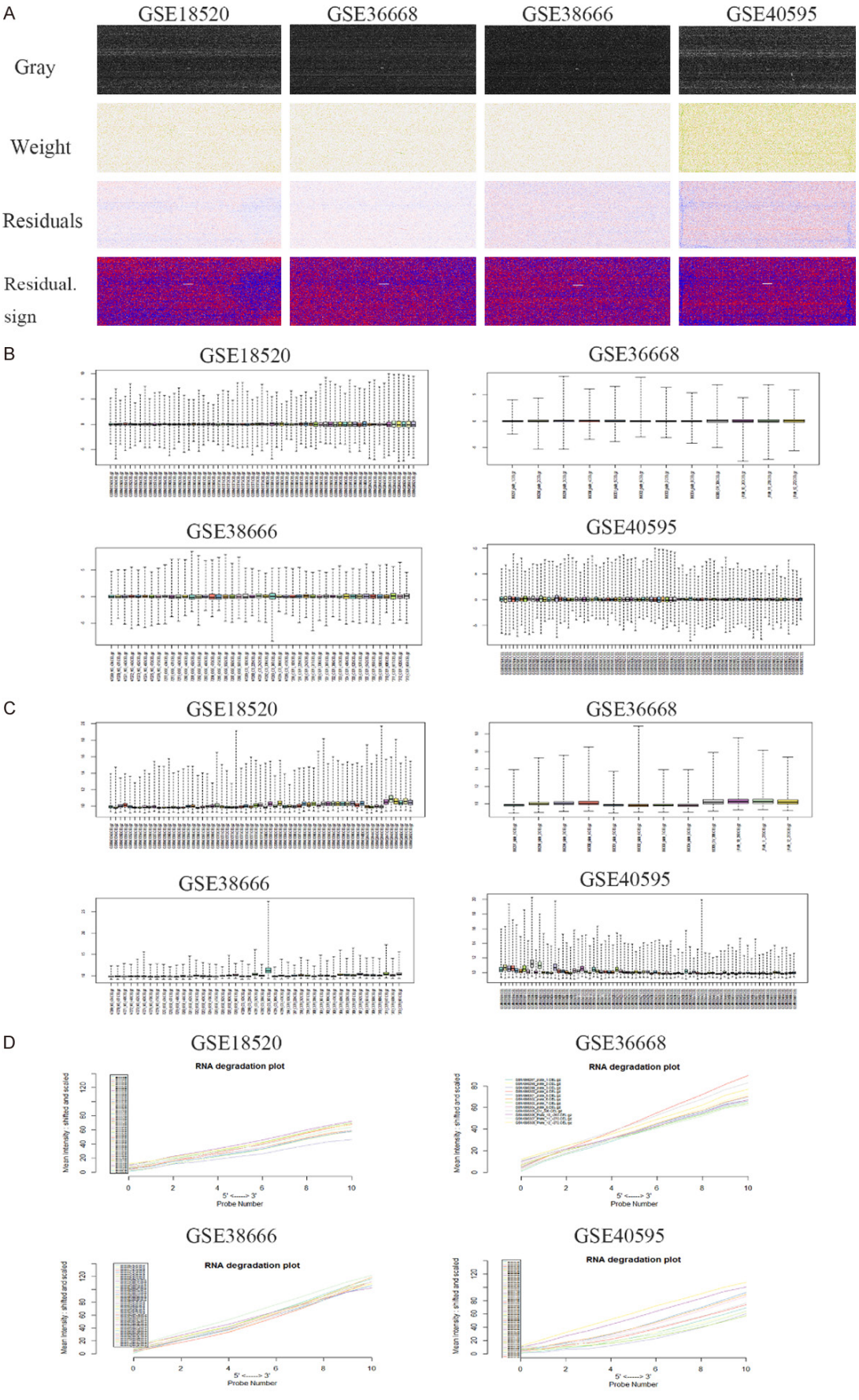
A
GSE18520
GSE36668
GSE38666
GSE40595
Gray
Weight
Residuals
Residual. sign
B
GSE18520
GSE36668
GSE38666
GSE40595
C
GSE18520
GSE36668
GSE38666
GSE40595
D
GSE18520
GSE36668
GSE38666
GSE40595
RNA degradation plot
Mean Intensity: shifted and scaled
5' <------> 3'
Probe Number

Figure S1. Quality detection of expression profiling of 4 OC genes (GSE18520, GSE36668, GSE38666 and GSE40595) downloaded from GEO. A. The gray, weight, residuals and residual sign plots of the selected datasets; B. Relative log expression (RLE) boxplots of the selected datasets; C. Normalized unscaled standard errors (NUSE) boxplots of the selected datasets; D. RNA degradation plots of the selected datasets.

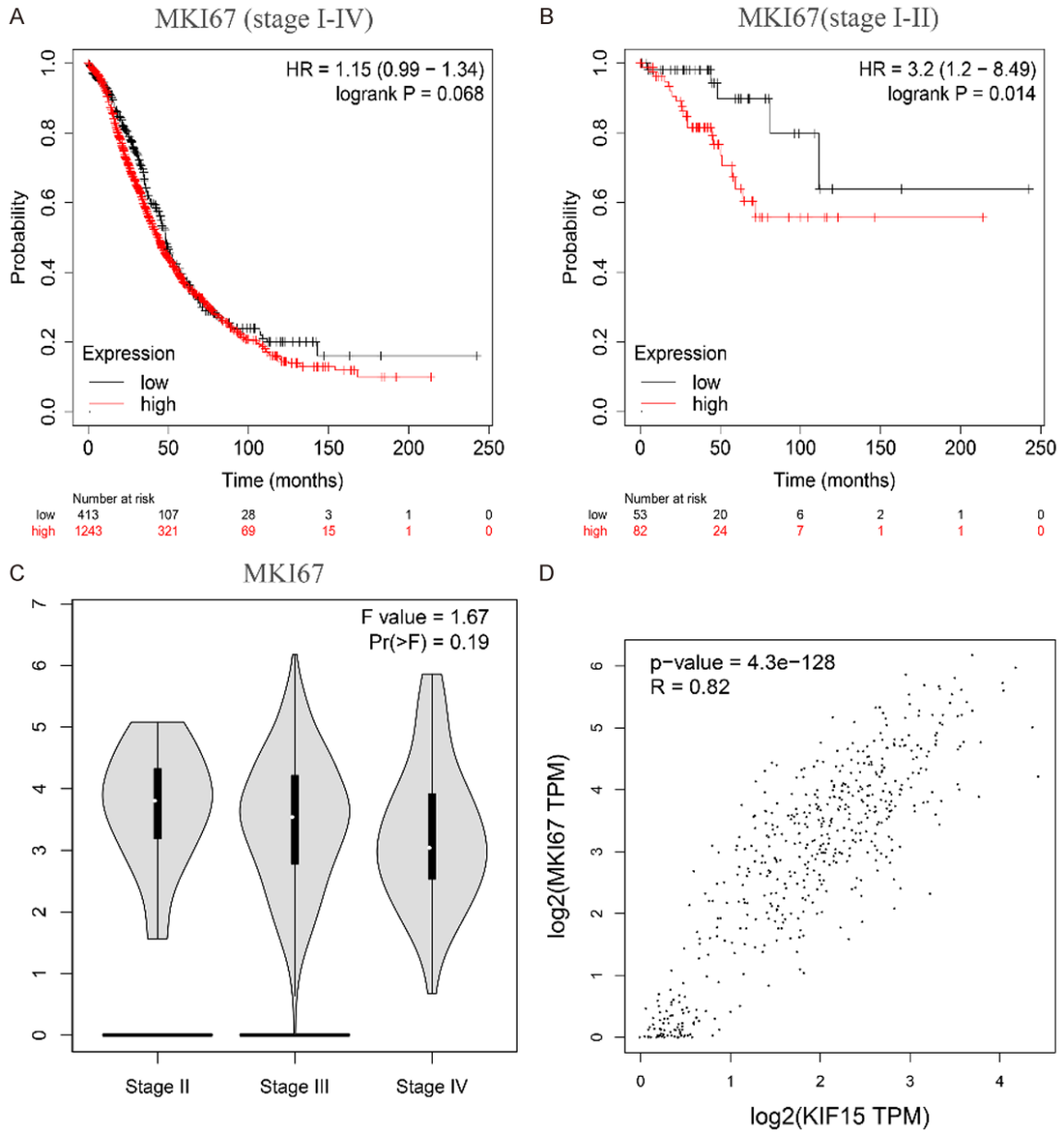

Figure S2. Bioinformatic analysis of MKI67 by using GEPIA online tool. A. Overall survival (OS) analysis of MKI67 on OC patients of stages I-IV; B. OS analysis of MKI67 on OC patients of stages I-II; C. Differential expression of MKI67 among stages; D. Correlation analysis of MKI67 and KIF15 using Spearman method.